People's Democratic Republic of Algeria

Ministry of Higher Education and Scientific Research

Kasdi Merbah University of Ouargla

Faculty of Hydrocarbons, Renewable Energies, Earth Sciences and the Universe

Renewable Energy Department

Thesis submitted for obtaining the degree of

Master

Specialty: Renewable Energies in Mechanics

Presented by:

AISSA GOUNNI

MOHAMMED HEYTHEM KHALED

MOHAMMED SEDDIK KOUIDRI

3D simulation of earth to air heat exchanger in Ouargla region

Thesis defended publicly 2021/2022

The jury members:

Dr. Maammeur Hocine	Chairman	Ouargla University
Dr.Belatrache Djamel	Supervisor	Ouargla University
Dr.Ammari Chouaib	Examiner	Ouargla University

College Year :2021/2022

Acknowledgements

Praise be to God Almighty, who enabled us to complete this scientific research

Our gratitude is great to our supervisor, **Dr. Belatrache Djamel**.

We extend our thanks to the members of the esteemed discussion committee.

To the Chairman**, Dr. Maammeur Hocine** and the examiner **Dr. Ammari Chouaib**, we would like to thank them warmly for their valuable advice and constructive criticism that brought this modest research work to an end.

And a heartfelt thanks to the Dean of the Faculty of Hydrocarbons, Renewable Energy, Earth Sciences and the Universe, Professor **Dr. Abdelmajeed Dobbi**, to the Head of the Renewable Energy Department, **Dr. Djamel Binmenin**, and to all the respected professors and professors from the Renewable Energy Department.

We say thank you very much for all your efforts**.**

إهداء

مرت قاطرة البحث بالعديد من العقبات. لكنني حاولت أن أتغلب عليه بثبات بفضل الله ومنه.

إلى **والديّ وزوجتي وابني هيثم وإخوتي وأصدقائي** ، فكانوا بمثابة سند ودعم لاستكمال البحث.

لا ينبغي أن أنسى **أساتذتي** الذين كان لهم الدور الأكبر في دعمي وتزويدي بالمعلومات القيمة....

أهدي لكم رسالتي...

سائلين الله تعالى أن يطيل أعماركم وأن يرزقكم بالخير.

عـيـسى قـنـي

إهداء

أحمد االله عز وجل على منه وعونه لإتمام هذا البحث.

إلى الذي وهبني كل ما يملك حتى أحقق له آماله، إلى من كان يدفعني قدما نحو الأمام لنيل المبتغى، **أبي** الغالي على قـلبي بارك االله في عمره؛

إلى التي وهبت فـلذة كبدها كل العطاء و الحنان، إلى التي رعتني حق الرّعاية و كانت سندي في الشدائد، **أمي** الحبيبة جزاها االله عني خير الجزاء.

إلى**إخوتي وأخواتي** الذين تقـاسموا معي عبء الحياة ؛

إلى **أهلي و أصدقائي** وكل من وقف بجانبي وساعدني بكل ما لديهم وبطرق عديدة.

أقدم لكم هذا البحث وآمل أن يرضيكم.

محمد هيثم خالد

إهداء

إلى والدي ووالدتي

إلى إخواني وأخواتي

لجميع الأساتذة في قسم الطاقات المتجددة جامعة ورقلة

إلى كل أهلي وأصدقائي

أقدم لكم هذا العمل المتواضع.

محمد الصديق قويدري

Figures list

Table list

Nomenclature

V	Fluid velocity [m/s]
Z	Depth of the ground [m]
Tout	Fluid temperature at the outlet of the pipe[°C]
L	Length pipe [m]
Pr	Number of Prandtl Dimensional
τ	The annul time period of temperature wave [s]
t	Time [day,s]
λ soil	Soil thermal conductivity [W/ m.°C]
d	Pipe diameter [m
P	Volumic mass [kg.m-3]
AS	Ground area temperature amplitude [°C]
$t_{0,s}$	phase constant, time of maximum surface temperature since the start of the year [day]
μ	Dynamic viscosity of the fluid [Pa. s]
β	The coefficient of thermal expansion
Cp	Capacity calorific [J/ (kg. °C)]
T_a	The ambient air temperature [°C]
A_a	The amplitude of the temperature oscillations e [°C]
G_k	The generation of turbulence kinetic energy due to the mean velocity
G_b	Is the generation of turbulence kinetic energy due to buoyancy
Y_M	The contribution of the fluctuating dilatation

Abbreviations

EAHE	Earth to air heat exchanger

Contents

Chapter 03: Results and discussions

GENERAL INTRODUCTION

General introduction

Global warming has become a major threat to the environment in recent years, particularly in arid and semi-arid areas, where the desert regions of southern Algeria recorded a significant increase in ambient temperature that exceeded the normal rate, it is a burden on the environment conventional air conditioners to meet the cooling needs of buildings during the summer .As a result, it is necessary to emphasize the use of new technologies based on Renewable energy still accounts for only 0.1 percent of Algerian energy consumption[1]. Energy consumption in urban buildings has recently increased in demand due to high comfort standards[2]. This energy accounts for approximately 40% of global energy consumption; for example, in Algeria, the residential sector is the largest consumer of energy, accounting for approximately 43% of total national energy consumption [3]. With population growth, urbanization, and improved living standards, this value will rise to 179.78 TWh in 2040[3] . Geothermal energy is a type of renewable energy. Heat is extracted from the earth and used for a variety of purposes including heating, cooling, bathing and therapeutic applications. It is also one of the few renewable energy sources that can be used indefinitely. Countries will be able to reduce their dependence on fuel imports and improve their energy security by producing electricity 24 hours per day and competing in cost with coal or natural gas. Deep geothermal resources remain mostly untapped. It is available on all continents, in addition to being environmentally friendly, it can be used repeatedly and is very effective[4]. To reduce the energy use required for heating and air conditioning. The use of EAHE (Earth to air heat exchanger) can be one of possible solutions to the problem of rationalizing energy use in the construction sector. Can It also helps reduce greenhouse gas emissions[5].

This work is divided into three chapters:

The first chapter is devoted to listing previous studies related to the topic, and in this part present a scenario and various implications for passive cooling, techniques used to reduce energy consumption and the efficiency of renewable energies. Also, present a bibliographical compilation of previous studies conducted by scientific researchers and construction specialists on thermal insulation systems; natural air conditioning by geothermal heat exchanger, heat pump and wind catcher.

The second chapter, present a mathematical model used to get the soil temperature used in Ouargla region at deferent depths. Then on optimal design factors for geothermal heat exchanger has been obtained by using Tagouchi method.

The third chapter is divided in to two sections, the first section contains the result of simulating the Earth's temperature at different depths in the Ouargla region, the second section contains the results obtained from simulating the geothermal heat exchanger for a whole year and during the winter and summer seasons.

In the end, a general conclusion was presented to finish this memory and arrive at the study results.

Chapter I

LITERATURE REVIEW ON PASSIVE COOLING SYSTEMS

1- Introduction

This chapter presents literature concerning three different techniques used for passive cooling. A bibliographical compilation of previous studies carried out by scientific researchers on passive cooling systems with its three techniques.

- Passive cooling systems use Earth to air heat exchanger;
- Passive cooling systems use Wind catchers;
- Passive cooling systems use heat pumps.

2- Passive cooling system use Earth to air heat exchanger

The first use the earth to air heat exchangers for air conditioning goes back a long way in time for heating and cooling agricultural buildings and greenhouses. The performance of an air/ground heat exchanger depends on the underground soil temperature, some researchers have experimentally studied the temperature of the subsoil, and others have used empirical models by estimation. Various numerical studies and experiments were carried out to estimate the variation of the temperature of the basement T (z, t) in the function of soil depth z and t. [6]

(Barakat et al., 2019) [7], Display and compare the new hybrid cooling system with other configurations of air-cooling systems within gas turbines. Cooling configurations include ground heat, air exchanger, fogging, and a new hybrid cooling system. From the results, the authors are noted that the hybrid system outperforms unitary systems because it can boost the average annual energy ground-air exchange system; respectively. The hybrid system reduces water consumption by 50 percent compared to the fog system. Moreover, the hybrid cooling system is the most effective method in areas with a temperature greater than 30 ° C.

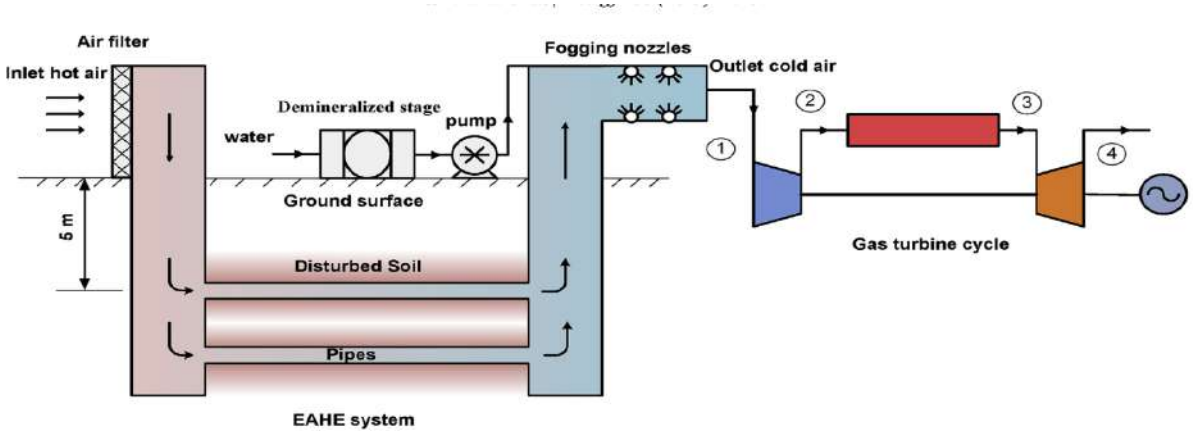

Figure I.1. Diagram of the proposed hybrid cooling system in a gas turbine[7]

(Gao et al., 2022)[8], present the impact of backfill on both heat and mass transfer of the EAHE system for deep underground emergencies offers ventilation. Results show that the impact of the backfill technology is almost important to the EAHE system in some cases, the successful deployment of the backfill system will help emergency ventilation in its process towards energy efficiency and thermal comfort, and the backfill system can further improve thermal performance by up to 10 % based on the original system. However backfilling is not a suitable method for the EAHE system under a depth of 400 meters.

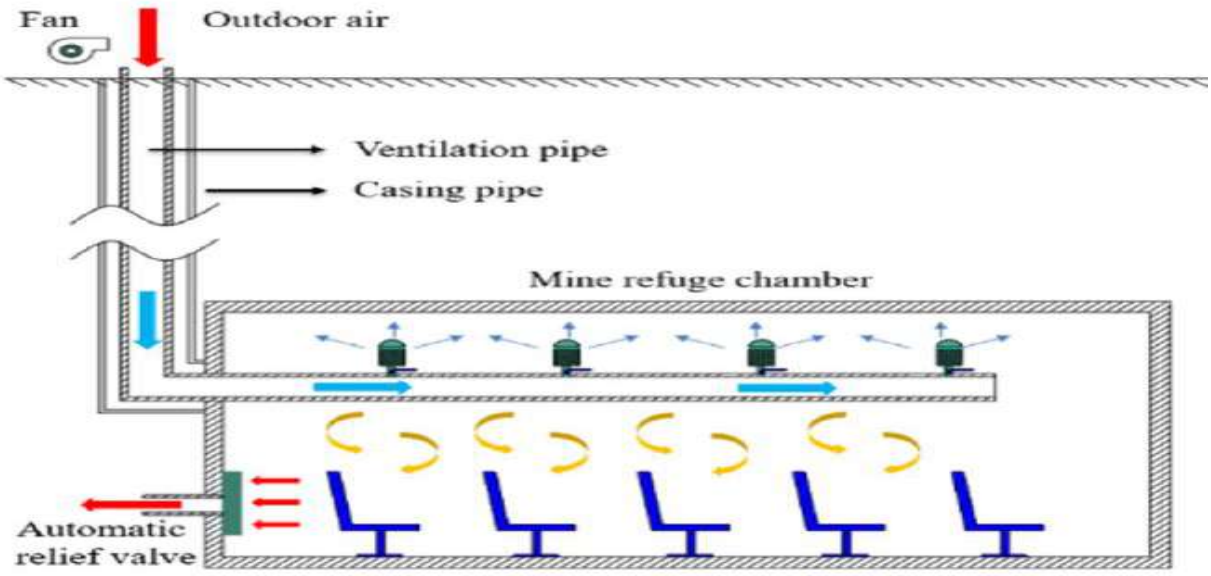

Figure I.2.deep underground chamber combined with a long EAHE system[8]

(Belloufi et al., 2022) [9], Presented EAHE Thermal Performance Inspection is offered in a continuous process. A transient digital model was developed using the implicit limitation thereafter, thermal performance was assessed using the heating agent method. To take measurements during cooling. Derating factors from 0% to 35% could mislead the EAHE design if ignored. The experimental results revealed that for 3.5 m/s of airspeed, the maximum air temperature can reach 19 °C. It is noted that the first 33 meters of the tube can provide 91% of the complete drop in air temperature. In extreme real cases, maximum air drop does not exceed 0.85 ◦C in 95 hours. Thus, the ambient temperature drops during night operation and then cooled the heated subsoil and helps the soil restore its cooling capacity.

(Li et al., 2019) [10] experimental work has been conducted, and the irrigation system has been adopted to empirically verify the impact of soil moisture content. The air temperature showed an average drop of 14.6 °C and the average total cooling capacity was 8792 watts. The system showed a maximum performance factor (COP) of 27.2, meaning that the system

provides fresh air cooling with little electricity input. Under cooling mode, the surrounding soil temperature has continuously increased due to the operation of the system. An irrigation system has been adopted to simulate natural rainfall; when soil humidity changed from 0.37 cm^3/cm^3 to 0.42 cm^3/cm^3, air temperature decreased by 1.6 ° C in the pipe outlet.

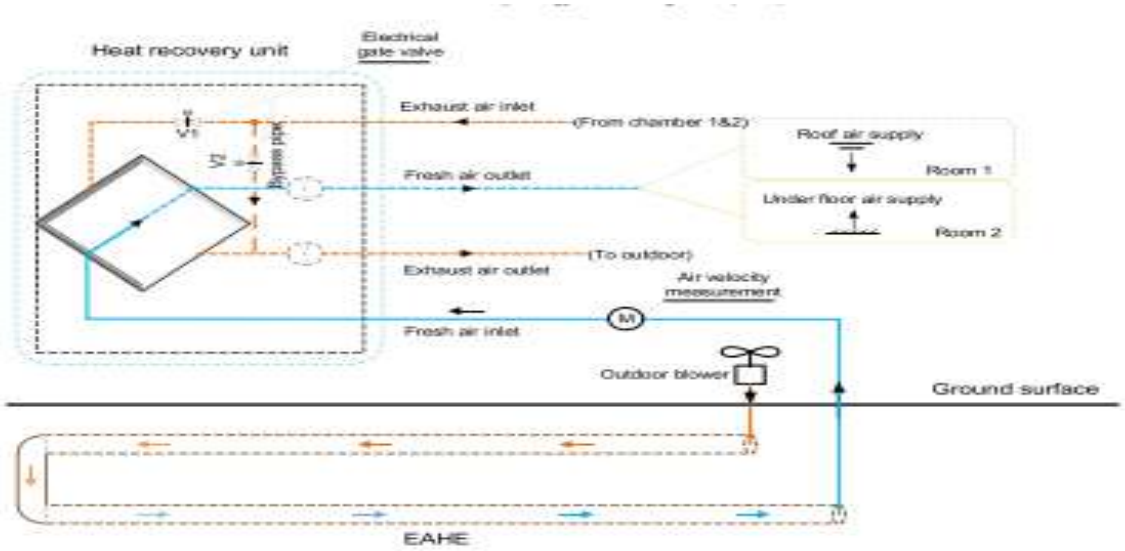

Figure I.3. Schematic diagram of the EAHE fresh-air supply system used in this study [10]

(Hegazi et al., 2021) [11], Study to determine optimal criteria for reducing the cost of central air conditioning in a hot and dry climate. A mathematical model was developed with the help of MATLAB to improve different parameters. The performance of the selected cooling system is assessed in terms of compressor power consumption, the maximum reduction of compressor power consumption is estimated at 44%.

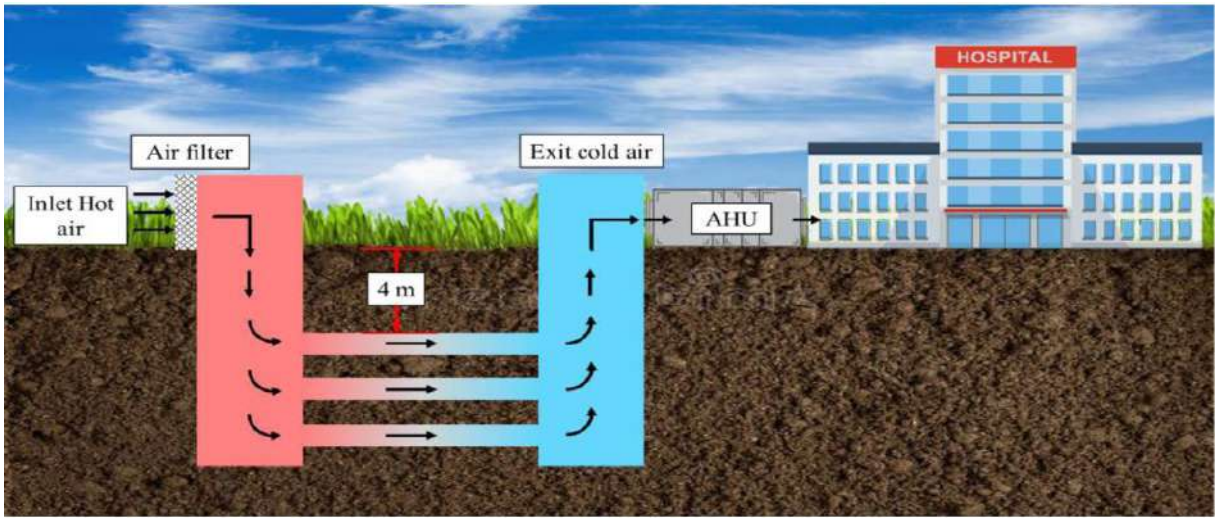

Figure I.4.Schematic diagram of the installation of EAHE system coupled with an AHU [11].

(Rouag et al., 2018)[12], Temperature distribution in the soil surrounding EAHE is studied in the target to determine the radius of the soil as a function of operating duration. This radius is the first distance from the pipe axis where there is no heat effect of EAHE. Therefore, a new transient semi-analytical model is being developed in particular to facilitate thermal design by applying extreme ambient air temperature results show that deterioration in EAHE thermal performance is observed longer in the hot climate. In the case of 6 hours of continuous operation, the soil radius can reach 0.55 meters from the tube surface.

3- Passive cooling systems use Wind catchers

(Calautit et al., 2020) [13], A suitable rotating heat recovery device was developed to integrate it with a multi-directional wind catcher system installed on the surface. In the first phase a full-range CFD prototype of the passive rotary heat wheel device was developed and tested in the cross-flow channel. Two configurations of the heat negative recovery wheel were tested: 20 and 32 radial blades. The second phase focused on investigating the integration of theheat recovery wheel into the wind hunter system. The results showed that the addition of a thermal recovery wheel rotating at 15 rpm reduced the speed of internal air flow between 14 and 30%, depending on external wind conditions.

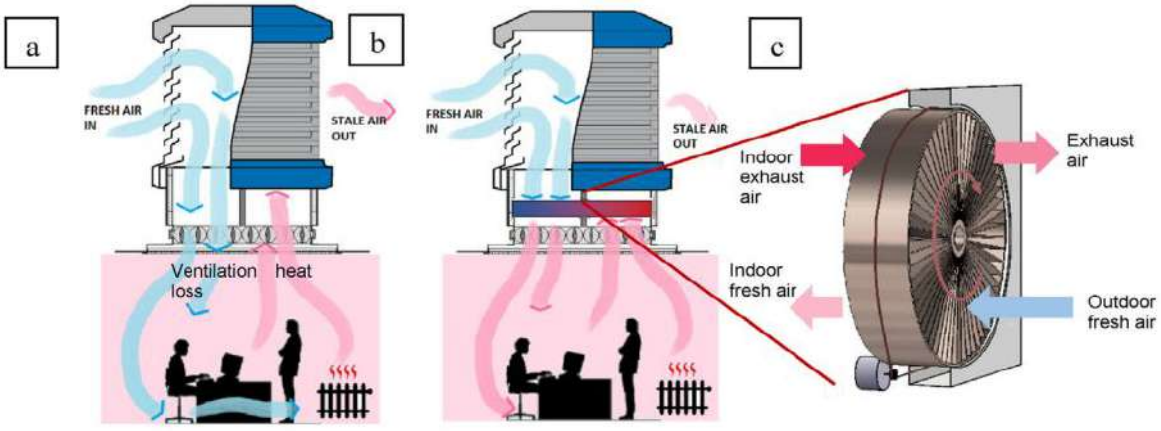

FigureI.5.(a) Standard wind catcher (b) passive heat recovery wind catcher (c) proposed passive heat recovery wheel.) [13]

(Zaki et al., 2019) [14], This study aims to analyze the flow behavior within the traditional two-side wind hunter building to better understand the impact of external air flow on internal ventilation behavior. The study was conducted experimentally in the wind tunnel and through CFD simulations using the standard disturbance model k- ε. The impact of different surface terrain and two different locations of the wind catcher building, below the tunnel floor with one wind catcher tower above the ground and above the tunnel floor were investigated.

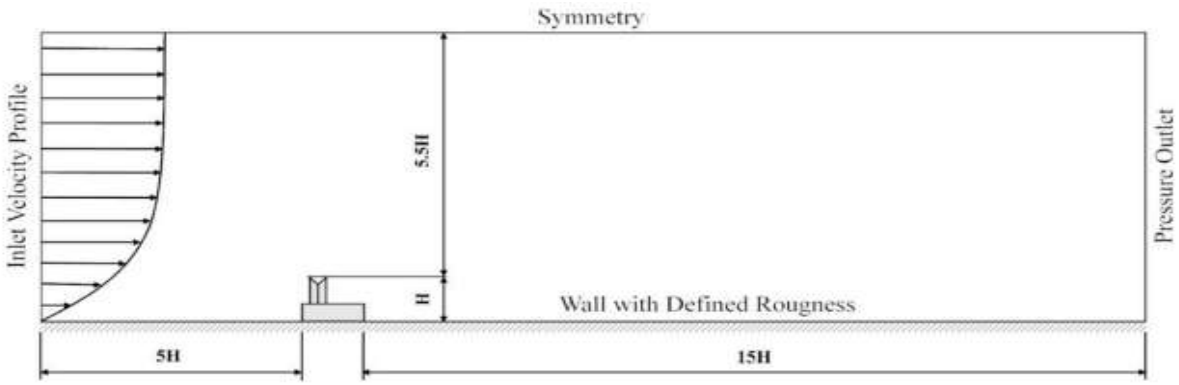

Figure I.6. Computational domain boundary conditions.[14]

(Sadeghi et al., 2020) [15], This study present three stages; first, the distribution of pressure on wind tower openings and building openings was measured in a boundary layer wind tunnel. Internal wholesale air flow change rates and average indoor room air speeds were derived. Second, the first phase pressure coefficient results were applied to the Sydney Model Meteorological Year (TMY) to assess the wind tower's ventilation performance in terms of internal air speed per hour. Wind tower results were measured against ventilation through the window. In the third phase, the increase in indoor air speeds under wind tower ventilation was processed by the Standard Efficient Temperature Comfort Model (SET *) to calculate additional rest degree hours resulting from wind tower insertion.

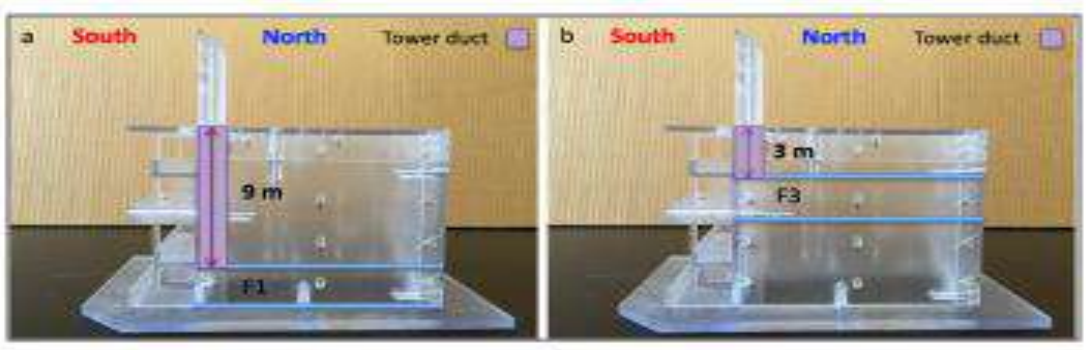

Figure I.7. (a) & (b). Building apartment model attached to wind towers [15]

(Goudarzi et al., 2021)[16], The internal flow structure, cross-ventilation characteristics, and thermal comfort of the built-in room are numerically investigated with a two-sided wind catcher. The 3D fixed state simulation RANS CFD is simulated, with different disturbance models for thereference state. Results show that the mass flow rate of the room port increases by up to 26% by reducing the height of the room port from top to floor; Floor and front outlet heights got optimal thermal comfort gauges. In a given room opening port, increasing the room outlet space to the wall ratio increases the mass flow rate; 30 % of the rise received the required temperature and speed range.

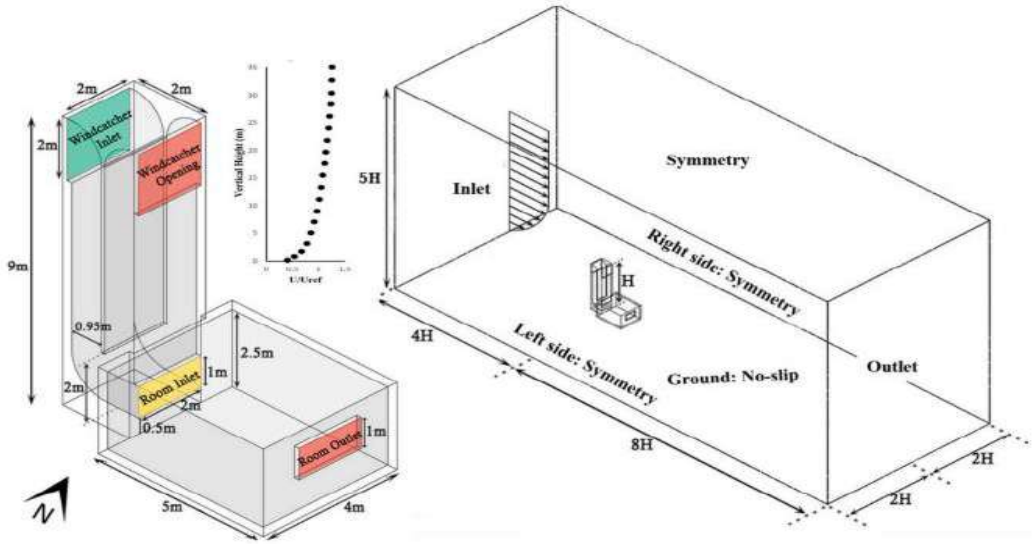

Figure I.8. Schematic of the reference case (left), computational domain with boundary conditions (right). [16]

(Ganesh et al., 2022)[17], . This study analyses the impact of the entrance diffuser direction (IDO) on the internal thermal comfort (ITC) of passengers and the energy demand in the building for indoor air heating. Different methods have been selected to study ITC for passengers such as air temperature... The results show that, with the uniform distribution of indoor air, the variation in the International Development Organization has a significant impact on ITC and energy consumption. Improving ITC can reduce indoor energy consumption by 35.14%.

(Miri et al., 2022) [18], two identical spaces, consisting of two interconnected rooms (collectively four rooms namely R1, R2, R3, and R4), were examined to assess the movement of dust and deposits in buildings. Rooms R1 and R2 had wind hunters facing the prevailing winds in the region, and R3 and R4 had wind hunters in the opposite direction of the prevailing

winds. Air speeds measured dust deposition density the results showed that air flow enters and leaves rooms R1, R2, and rooms R3 and R4 respectively.

(Mohamad abadi et al., 2018) [19], The numerical study was conducted on a scale model of 1:25 for 13 wind accident angles of 15 degrees. Interesting parameters were the flow rate and the ratio of total extract to supply flow rates at each angle from the angle of wind accidents. An organized network was established, and ANSYS Fluent was used to simulate the flow field. A wind tunnel experiment was conducted on the same scale model and a semi-experimental approach was adopted to predict the rate of airflow at each wind corner.

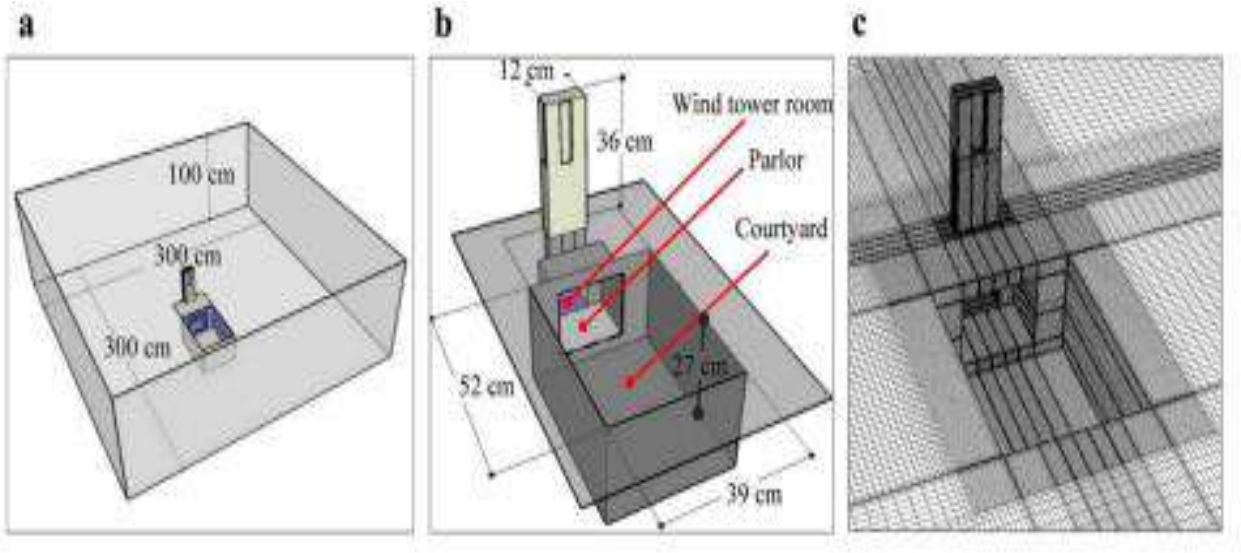

Figure I.9.(a) Computational domain for the simulation of external wind; (b) the wind tower and the building model; (c) computational grid[19].

(Alwetaishi & Gadi, 2021) [20], The study focuses on investigating new and innovative forms of wind hunters to improve air speed indoors which will raise indoor comfort and air quality in buildings. The study used CFD computer modeling and a real model experiment to conduct the study. The study highlighted that curved shapes have the highest pattern of driven wind speed, especially curved shapes with double entrances. The study showed that the octagon shape has the lowest pattern of wind speed driven due to its different aspects that prevent air flow easily inside the tunnel.

(Pakari & Ghani, 2019) [21], Air change rate and air flow distribution within a greenhouse equipped with wind towers are analyzed using CFD, taking into account wind speeds. The systems showed fair agreement. The average discrepancy between hot wire speed measurements and simulation results was about 7.96%. Expected tanker fields in wind towers showed good agreement with corresponding PIV measurements. The discrepancy between maximum speed and air measurement in the entrance tower was 15%, while 3% was in the outlet wind tower. With an external wind speed of 3 m/s and a natural angle of occurrence, the average air flow to the greenhouse was 0.65 m/s, while the average air speed in the greenhouse was 0.44 m/s.

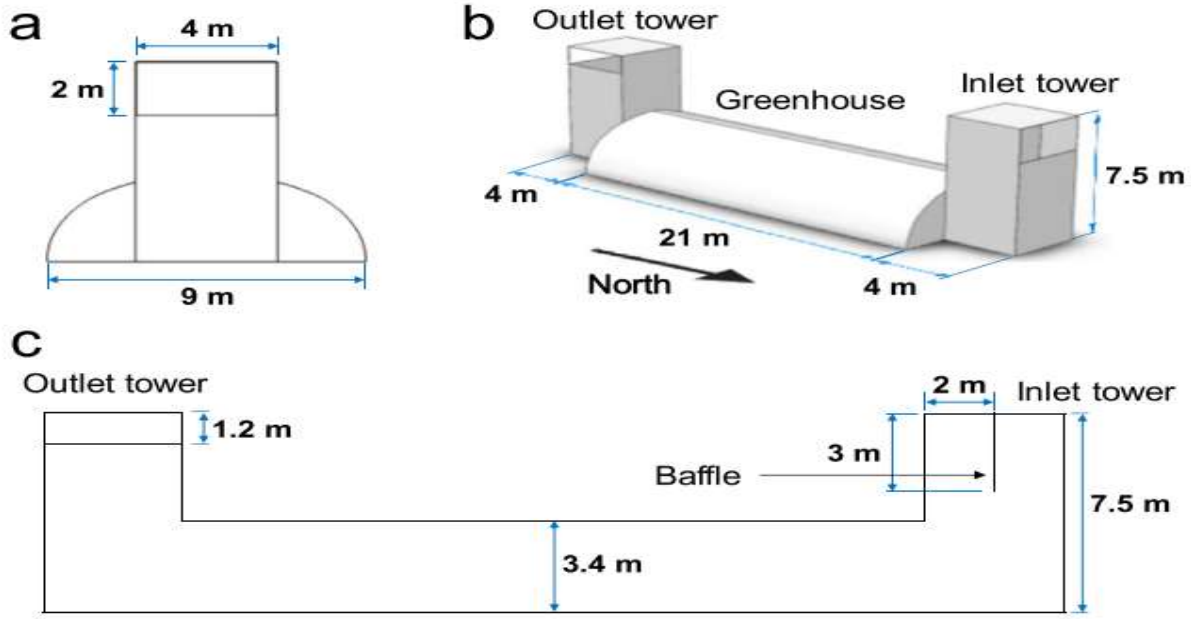

Figure I.10.Greenhouse incorporating two wind towers: (a) side view, (b) perspective view, and (c) front mid-plane section view. [21]

(Yang et al., 2019) [22], The study offers the relative ventilation relationship of rooms in the "line" type middle school teaching building. Several parameters such as indoor and outdoor corridors, different room sizes and, different ventilation angles are assigned as variables, using a CFD simulation method. The combined and separate effects of the parameters set on natural ventilation performance are assessed using the atmospheric area ratio as criteria. The result shows that the "line" type teaching building with external corridor ventilation is 35.55% better than the inner corridor. Ventilation in the large room is 30.84% better than those in small rooms, the best wind angle for ventilating buildings.

(Jafari & Kalantar, 2022)[23], It provides an assessment of the evaporative refrigeration rate in a building in a hot climate, the windcatcher is coupled with three solar chimneys, and the water spray system (WSS) to lower the temperature we use CFD to simulate the system proposed. The effect of variables is studied using ANSYS FLUENT software. The study highlighted that adding WSS leads to a drop of approximately 6-12 ° C in temperature; moreover, relative humidity will rise by 80% on the third floor.

4- Passive cooling systems use heat pumps

(Jahangir & Labbafi, 2022)[24], Study ground source thermal pump system with energy storage energy, to improve the performance of open microalgae transplant system, results are calculated and measured for heating (coldest month per year) and cooling (hottest month per year). The relationships between results and variables are obtained, concluding that the cooling mode has a 48.7% higher performance factor and a 54% increase in weekly microalgae production compared to one GSHP system. Similarly, heating mode causes a 53.7% increase in performance coefficient and a 27.6% increase in microalgae production rate.

(Biglarian & Abdollahi, 2022)[25], Introducing the PV-GSHP hybrid system feasibility of a building. A digital model was developed to explore the performance of the GSHP system over 20 years of design. The results show that the use of four (04) photovoltaic units can best cover the system's electricity consumption and the reduced recovery period is less than four years.

(Hu et al., 2022)[26], This study shows the cooling performance of the genuine hybrid recovery geothermal pump system along with thermally activated construction systems in a residential area. The hybrid ground source system with cooling tower has improved the operating performance, increased energy efficiency and these services cannot be utilized in the use of low energy. Thus, a multiple temperature power system is recommended.

(Luo et al., 2022 [27], present a hybrid system integrating a thermal pump from a terrestrial and anaerobic source (GPAD) for rural buildings, a two-stories house was selected that compared two traditional scenarios, including geothermal pump systems (GSHP) and air source thermal pump system (ASHP), to the GPAD system. The results showed that the annual energy efficiencies in the three scenarios were 3.66 (GSHP), 2.54 (ASHP) and 4.17 (GPAD) respectively; The GPAD system showed higher efficiency, which was 14.0% higher than the GSHP system and 64.1% higher than the ASHP system.

(Nordgård-Hansen et al., 2022) [28], the present work Separate residential homes,

where the energy system consists of photovoltaic systems for energy generation and batteries and optional ground-source heat pump systems for energy storage. It is also found that ground-source heat pump systems contribute to increased sustainability, but they may not be economically useful for homes with low or medium heating requirements. As well as areas available for photovoltaic power generation and externally available power sources. Therefore, a detailed analysis of the type presented here is recommended before the implementation of new energy policies.

(Liu et al., 2019)[29], present a simulation model for GSHP system, the authors studied the performance of hybrid GSHP system with cooling tower HGSHP then the variation was calculated for one and 10 years and the results shown that the average annual electricity consumption of the HGSHP system decreased by 6 .40% and the performance coefficient increased by 7 .12% during the first year of operation. In addition, the temperature of the buried pipe outlet was less than 32 ° C for the HGSHP system during a ten-year operating period, while in the GSHP system, the standard excess temperature of the buried pipe outlet can reach approximately 80% and the soil temperature increased by 10.9 ° C. So HGSHP can provide a feasible solution for cooling and heating.

(Lee et al., 2022)[30], The heating performance of GSHP and SGSHPs is analyzed in a heating-dominated building and compared for 20 years by changing the length of the well and solar collection area. With a well length of 120 meters and a solar collector area of 10 square meters, SGSHP showed a 12.6 and 11.5 % higher ground temperature and sun collector efficiency, respectively. However, SGSHP with parallel configuration reduced energy consumption by 19.6 and 13.8% compared to those for the GSHP and SGSHP with a serial configuration.

(Shimada et al., 2021) [31], Evaluated the energy performance of the GSHP system in representative construction models based on operating conditions derived from the temperature of the heat basin expected for 50 years. The proposed system combines GSHP with air source heat pump (ASHP), and in one scenario, GSHP also provides hot water. The results confirm that the common system achieves higher efficiency than those found in the ASHP system alone, and that the GSHP provides hot water achieves significant energy savings. However, restrictions on annual GSHP operating hours are necessary, resulting in reduced energy-saving performance of refrigeration-dominated facilities. Further improvements are expected by mitigating thermal interactions between each well heat swap.

(Violante et al., 2022) [32], A comparative assessment of the life cycle of an experimental GSS system was conducted, the impacts on the four damage criteria were evaluated for each phase of the entire life cycle (production, installation, operation and end-of-life)with slightly higher effects recorded for the ASHP system. The shelf life of the geothermal probe circuit is 100 years, allowing multiple operational life cycles of the geothermal plant. ASHP is more energy efficient and has less long-term environmental impact, compared to traditional air conditioning system.

(Naili & Kooli, 202) [33], checked the feasibility of a solar-assisted geothermal pump system (SAGSHP), this system consists of a ground source thermal pump (GSHP) with horizontal geothermal exchanger and buried tank, and solar flat plate collector (SFC) as an auxiliary thermal source. Two forms have been developed and technically evaluated. Heating space by SFC only, and SAGSHP. The results show that the independent SFC heating increases the internal air temperature by about 3 ◦C, but it does not guarantee thermal comfort (22 ◦C), and the lab SAGSHP achieves significant high performance to heat the place. Serious analysis proves the high performance of the SAGSHP system, and economic assessment shows a good cost benefit for this system.

(Zhou, Mao, Li, et al., 2022) [34], This study highlights the importance of using horizontal GSHP methods to improve thermal and economic performance. Two modes of variable flow regulation, (SFC and TFC), along with (CFC), were used in the secondary episode of the system. The three-dimensional numerical model of HGHE was built considering the cellular porous soil and various environmental ambient conditions and coupled with the heat pump model for heating analysis and economic efficiency of the horizontal GSHP system. Given that the buried depth of HGHE, H, may vary in different conditions, the effect of flow control methods in different H. results reveal that the difference range in fluid temperature between the input and outlet of HGHE, Δ TF, COP system, COPsys, is smaller and TF level Δ and COP SYF System operating costs and electricity charge ratio in water pump can decrease by up to 9.80% and 47.26%, but the differences between variable flow control technologies are not significant.

Conclusion

From previous studies and research, which treated passive cooling methods in various forms, it is noted that passive cooling systems use Earth to air heat exchanger, use Wind catchers and use heat pumps are important to reduce temperature and reduce electricity consumption in homes.

Chapter II

Modeling and methods

1. Introduction

This chapter aims to establish a mathematical model to determine the soil temperature at different depths and the air temperature at the outlet of the exchanger.

In common heat exchangers, two fluids different temperatures are in motion from the inlet to the outlet[35, 36]. In the case of an air-ground exchanger, one of these sources is the air circulating in the buried pipe, the other is the ground placed in contact with the tubes[37].The latter plays the role of the cold source during the hot season, and the hot during the cold season. So, the temperature of the air at the inlet of the tubes and the temperature of the ground constitutes the boundary conditions for the exchanger.

The air temperature at the inlet of the exchanger corresponds to the temperature of the outside air; it is easily measurable or accessible from hourly meteorological databases. On the other hand, the temperature of the undisturbed soil cannot be known without the use of a measuring device that is difficult to implement (thermal probe placed at thesoildepth). There is no database that can provide this temperature, which is why modelling seems necessary, in order to obtain the ground temperature at any time and at any depth[37]

2. Problem Description

Natural ventilation was previously used in the architecture of traditional cities in south Algeria[38] Passive cooling techniques have become more appealing in recent years, which justifies their use under various conditions, to reduce the use of electricity in air conditioning devices and the use of CFC, which contribute to global warming[39]. Furthermore, the ground contains a significant thermal potential (geothermal energy) that can be used in air conditioning. The recovery of thermal energy from the ground is primarily accomplished using buried heat exchangers[40]

EAHE is made up of a tube length or a network of buried pipes at a reasonable depth below the ground's surface. The supply of ventilation air is routed through pipes, and the temperature difference between the pipe surface and the air drives the heating/cooling of ventilation air. The magnitude of heat exchange between air and pipe is affected by variables such as soil temperature. Air temperature, pipe dimensions, airflow rate, pipe burial depth, soil and pipe thermal conductivity are all factors to consider. The EAHE has the potential to eliminate the need for active mechanical and air-conditioning units in buildings, resulting a significant reduction in electricity consumption

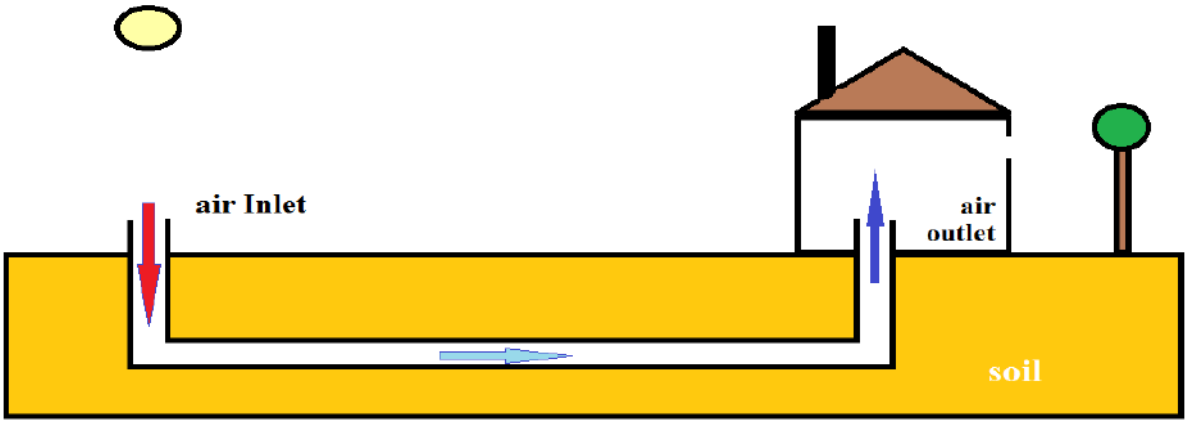

Figure II. 1.Schematic diagram of a passive air-conditioning system using earth air heat exchanger

2.1. Physical models

2.1.1. Model of the semi-infinite massif

A semi-infinite solid is a perfect body with a single flat surface that extends to infinity in all directions. If the variety of a thick wall is what we're after, may represent it as a semi-infinite medium. [41].

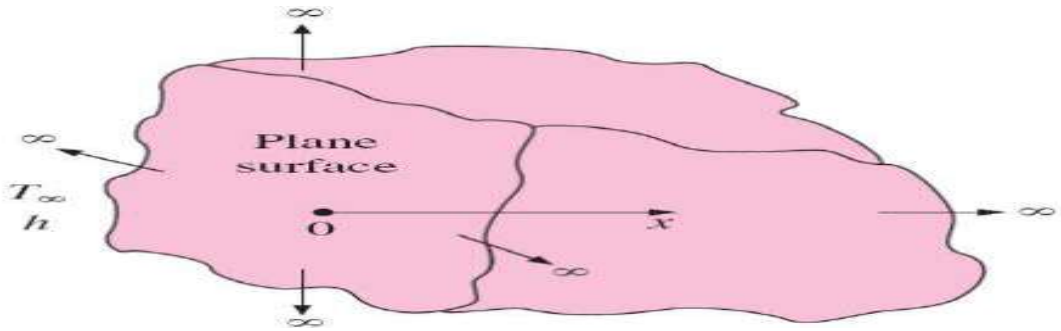

Figure II. 2.Schematic of a semi-infinite body[41].

In determining temperature variations near its surface, the earth can be thought of as a semi-infinite medium surface

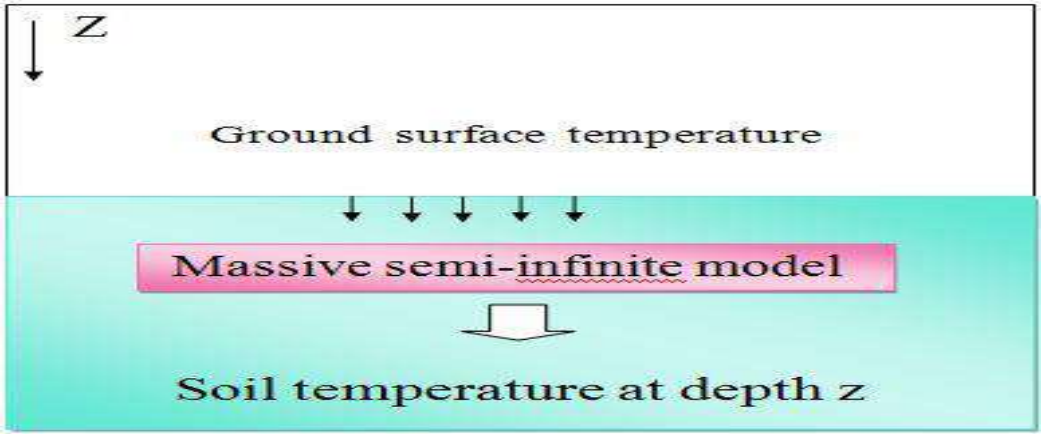

Figure II. 3. Massive semi-infinite model.

2.1.2. Modelling of the soil temperature

The assessment of geothermal potential using buried/ground air heat exchanger technology necessitates the determination of year-round changes in the temperature of the Earth at various depths. These differences are obtained through simple modelling that considers Earth's characteristics and ambient temperatures. A quasi-empirical relationship describes the evolution of the external ambient temperature as a function of time (day). The following expression expresses the relationship that governs the change in soil temperature[42].

The ambient air temperature, T_a can be expressed as a periodically signal according to the relationship [43].

$$T_a(t) = \bar{T_a} + A_a \times \cos\left(\frac{2\pi(t - t_{0,a})}{365}\right) \quad (1)$$

With [43].

$$\bar{T_a} = \frac{1}{365}\int_1^{365} T_a(t)\,dt \quad (2)$$

The amplitude of the temperature oscillations A_a is [43].

$$A_a = \frac{T_{a\max} + T_{a\min}}{2} \quad (3)$$

The ambient air temperature is easily measurable or accessible from weather databases.

On the hand, the soil temperature cannot be known without the use of a thermal probe placed at the soil [44].

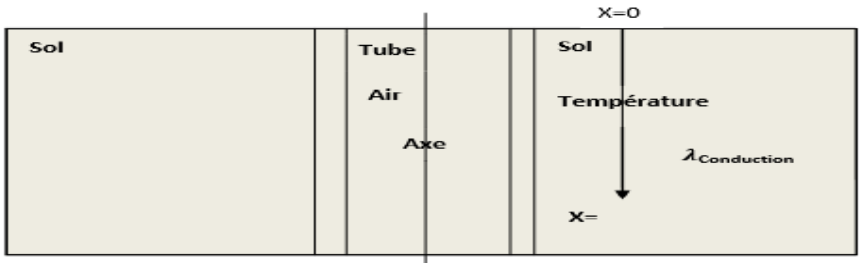

Figure II. 4.Schematization of the Physical Problem[45]

$$\frac{\partial T(z,t)}{\partial t} = a_s \times \frac{\partial^2 T(z,t)}{\partial z^2} \quad (4)$$

Applied to the semi-infinite soil with boundary conditions $T(\infty,t)$ is finite for the infinite depth soil.

For $z = \infty : T(\infty,t) = T_s$ (5)

Have the following from solution for calculating the temperature $T(z,t)$ of the soil, At time t and depth z [43].

$$T(z,t) = \bar{T_s} + A_s \times e^{-\frac{z}{d}} \times \cos\left(\frac{2\pi(t - t_{0,s})}{365} - \frac{z}{d}\right) \quad (7)$$

Where [43]]

$$d = \sqrt{\frac{a_s \times \tau}{\pi}} \quad \text{And} \quad a_s = \frac{\lambda_s}{(\rho_s \times C_s)} \quad (8, 9)$$

$t_{0,s}$: phase constant, time of maximum surface temperature since the start of the year (days).

τ : The annul time period of temperature wave (s) .

2.2. Hypotheses

To formulate the problem mathematically, the following assumptions must first be made:[46]

- The soil around the pipe is isotropic, with uniform thermal conductivity across all ground strata;
- One-dimensional air flow on the x-axis with constant properties
- The pipe material's thermal resistance is negligible (thickness of the pipe is very small);
- The ground's surface temperature can be approximated to the ambient air temperature, which is equal to the inlet air temperature;

- The pipe has a circular cross-section;
- After a distance of 'r' from the pipe's outer surface, the thermal effect of the soil surrounding the pipe is negligible, where 'r' is the pipe radius.

By taking into account the above hypotheses, the heat conduction and energy equations in the two-region (soil-air) domain can be written respectively [47].

2.3. Governing equations

The following set of governing equations is used to simulate heat and mass transfer and fluid flow in any system using FLUENT software[48].

- The equation for the mass conservation law [48].

Also known as the continuity equation, is written as

$$\frac{\partial u}{\partial x}+\frac{\partial \nu}{\partial y}+\frac{\partial w}{\partial z}=0 \tag{10}$$

- Law of energy conservation:[48].

The first law of thermodynamics or law of energy conservation stated as neither the energy can be created nor destroyed, it only changes its form in nature. The equation can be written as follows[48]:

$$u\frac{\partial T}{\partial x}+\nu\frac{\partial T}{\partial y}+w\frac{\partial T}{\partial z}=\alpha\left[\frac{\partial^2 T}{\partial x^2}+\frac{\partial^2 T}{\partial y^2}+\frac{\partial^2 T}{\partial z^2}\right] \tag{11}$$

- Law of momentum conservation (Navier–Stokes equation, also known as Newton's second law)[48]:

The equation for momentum conservation is as follows:

X-momentum equation

$$u\frac{\partial u}{\partial x}+\nu\frac{\partial u}{\partial y}+w\frac{\partial u}{\partial z}=-\frac{1}{\rho}\frac{\partial p}{\partial x}+\nu\left[\frac{\partial^2 u}{\partial x^2}+\frac{\partial^2 u}{\partial y^2}+\frac{\partial^2 u}{\partial z^2}\right] \tag{12}$$

Y-momentum equation

$$u\frac{\partial v}{\partial x}+v\frac{\partial v}{\partial y}+w\frac{\partial v}{\partial z}=-\frac{1}{\rho}\frac{\partial p}{\partial x}+\nu\left[\frac{\partial^2 v}{\partial x^2}+\frac{\partial^2 v}{\partial y^2}+\frac{\partial^2 v}{\partial z^2}\right] \quad (13)$$

Z-momentum equation

$$u\frac{\partial w}{\partial x}+v\frac{\partial w}{\partial y}+w\frac{\partial w}{\partial z}=-\frac{1}{\rho}\frac{\partial p}{\partial x}+\nu\left[\frac{\partial^2 w}{\partial x}+\frac{\partial^2 w}{\partial y^2}+\frac{\partial^2 w}{\partial z^2}\right] \quad (14)$$

In the preceding Eqs(12.13.14), u, v, and we are the velocity components in the x-, y-, and z-directions, respectively, and T and P are the temperature and pressure of the flowing air.

- Energy equation:

$$\frac{\partial}{\partial_t}\left(\rho C_p T\right)=\frac{\partial}{\partial x_i}\left(k\frac{\partial}{\partial x_i}-\rho\overline{u'T}\right) \quad (15)$$

2.4. Turbulence models

Within the model, the k-ε transport equation is used to define the turbulence kinetic energy and flow dissipation rate. It is the most basic turbulence model, requiring only initial or boundary conditions to be applied. Furthermore, it is the most widely used and validated turbulence model. In this equation, k denotes the kinetic energy of turbulence and s denotes the rate of dissipation. The equations can be written as follows[49].

$$\frac{\partial}{\partial t}(\rho k)+\frac{\rho}{\partial x_i}(\rho k u_i)=\left[(\mu+\frac{\mu_i}{\sigma_k})\frac{\partial k}{\partial x_j}\right]+G_K+G_b-\rho\varepsilon-Y_M+S_K \quad (16)$$

And

$$\frac{\partial}{\partial t}(\rho k)+\frac{\partial}{\partial x_i}(\rho\varepsilon u_i)=\frac{\partial}{\partial x_j}\left[\left(\mu+\frac{\mu_t}{\sigma_\varepsilon}\right)\frac{\partial\varepsilon}{\partial x_j}\right]+G_{1\varepsilon}\frac{\varepsilon}{k}\left(G_k\ C_{3\varepsilon}G_b\right)-C_{2\varepsilon}\rho\frac{\varepsilon^2}{k}+S_\varepsilon \quad (17)$$

G_k :Represents the generation of turbulence kinetic energy due to the mean velocity gradients ; calculated as [49].

$$G_k=-\rho\overline{u_i u_j}\frac{\partial u_j}{\partial x_i} \quad (18)$$

G_b :Is the generation of turbulence kinetic energy due to buoyancy ,calculated as [49]:

$$G_b=\beta g_i\frac{\mu_t}{p_{rt}}\frac{\partial T}{\partial x_i} \quad (19)$$

P_{rt} : Is the turbulent Brandt number for energy and g_i is the component of the gravitational vector in the direction.

β : The coefficient of thermal expansion.

Y_M : Represents the contribution of the fluctuating dilatation in compressible turbulence to the overall dissipation rate, calculated as[49]:

$$Y_M = 2\rho M_t^2 \text{Mach number} M = \sqrt{\frac{k}{a^2}} \quad (20)$$

The model constants $C_{1\varepsilon}$ and C_2 , σ_k and σ_ε are the turbulent Brandt numbers for k and ε .

S_ε And S_k are user –defined source terms Modelling of turbulent viscosity:

$$\mu = \rho C_\mu \frac{K^2}{\varepsilon} \quad (21)$$

$C_{1\varepsilon} = 1.44$; $C_{2\varepsilon} = 1.92$; $\sigma_k = 1$; $\sigma_\varepsilon = 1.3$; $C_\mu = 0.09$

2.5. Boundary conditions

Setting the proper boundary conditions is a critical step in any numerical study. These boundary conditions must be very close to the reality of the physical phenomenon being studied. However, due to the complexity, boundary condition simplifications are required. For EAHE applications, where the Mach number does not exceed 0.3, because air velocity is typically quite low compared to sound speed. As a result, the flow is regarded as incompressible, its properties are regarded as constants. The boundary conditions used in this study are summarized below.[50]

- **Velocity inlet**: at the inlet of the EAHE pipe, the velocity can be assumed constant.
- **Outflow**: in the outlet boundary, were the pressure and temperature are not known, the outflow boundary condition is more suitable for this case. This boundary applies a zero-flux normal to the outlet surface for compute all problem variables.
- **Wall**: for the wall of the pipe and for the soil domain, the wall boundary condition has been utilized, this applies a no-slip condition (velocity null) at the pipe wall. For the soil, a constant temperature has been applied (undistributed temperature T0)

2.6. Mesh choice

Mesh generation (2D or 3D) is a very important phase in a CFD analysis, given the influence of its parameters on the calculated solution. This menumakes it possible to mesh in particular a line of the geometry, namely to lay out thenodes with particular conditions (use of a ratio to modify themesh weighting, application of different mesh shapes)[51]

a. Structured mesh (quadra/hexa)

It is much easier to generate it using a geometry with multi block, it has the following advantages:

• Economical in number of elements, presents a lower amount of mesh per compared to an equivalent unstructured mesh.;

• Reduces the risk of numerical errors because the flow is aligned with the mesh. Its disadvantages;

• Difficult to generate it in the case of a complex geometry;

• Difficult to obtain a good mesh quality for certain geometries Complex.

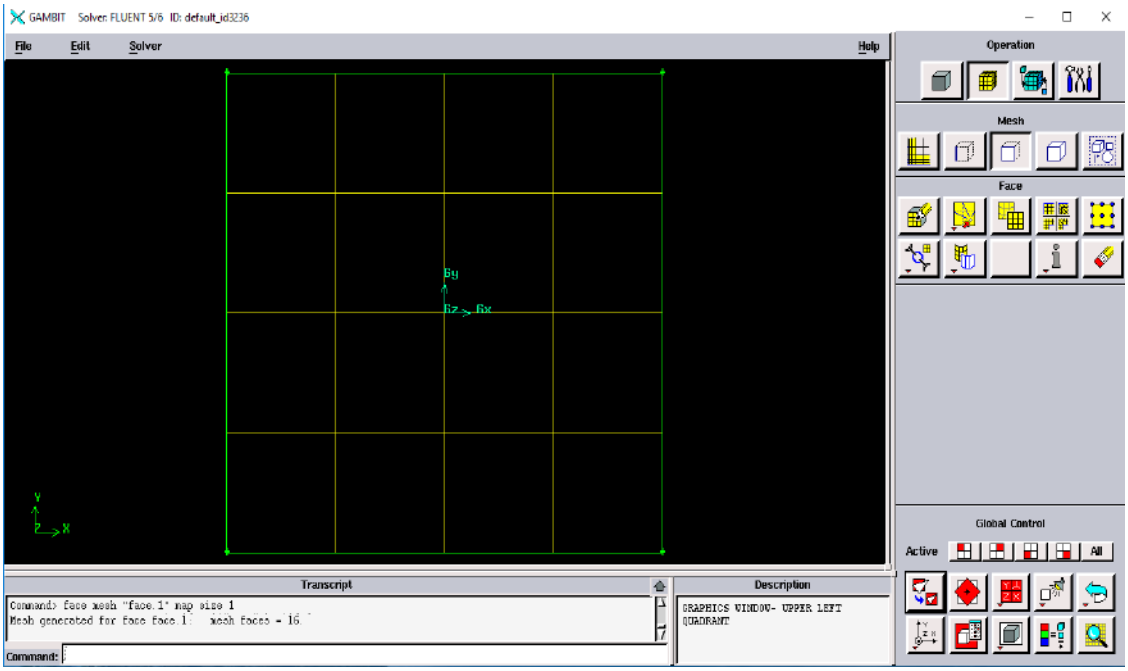

Figure II. 5.structured mesh (quadra/hexa)

b. Unstructured mesh (tri/tetra)

The elements of this type of mesh are generated arbitrarily without any constraints on their disposition. His advantages:

• Can be generated on complex geometry while maintaining good quality elements.

• The generation algorithms of this type of mesh (tri/tetra) are very automated its disadvantages:

• Very greedy in number of meshes compared to the structured mesh;

• Generates numerical errors (false diffusion) which can be more important if we compare with the structured mesh;

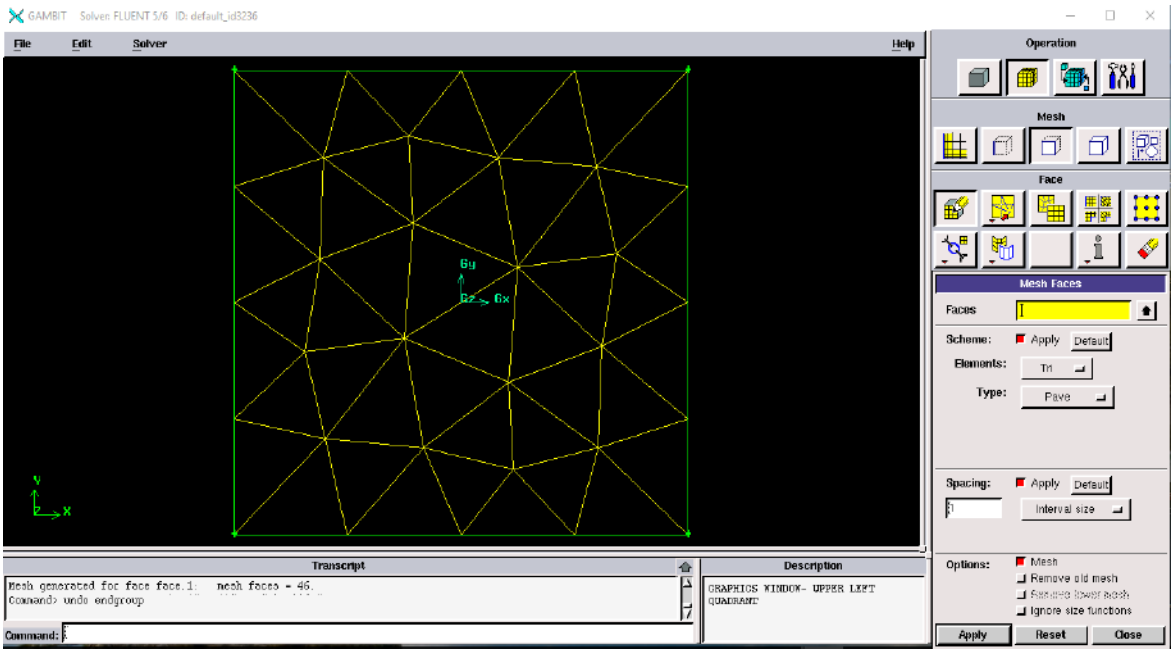

Figure II. 6. Unstructured mesh (tri/tetra)

c. Hybrid Mesh

Mesh generated by a mixture of elements of different types, triangular or quadrilateral in 2D, tetrahedral, prismatic, or pyramidal in 3D. His advantages combine the advantages of the structured mesh and those of the unstructured mesh.

- Fast and easy to prepare (in a few minutes);
- Fast to calculate;
- Very accurate to follow the real part shape;
- Matching perfectly the requests of the solver [52]

2.7. The computational Domain

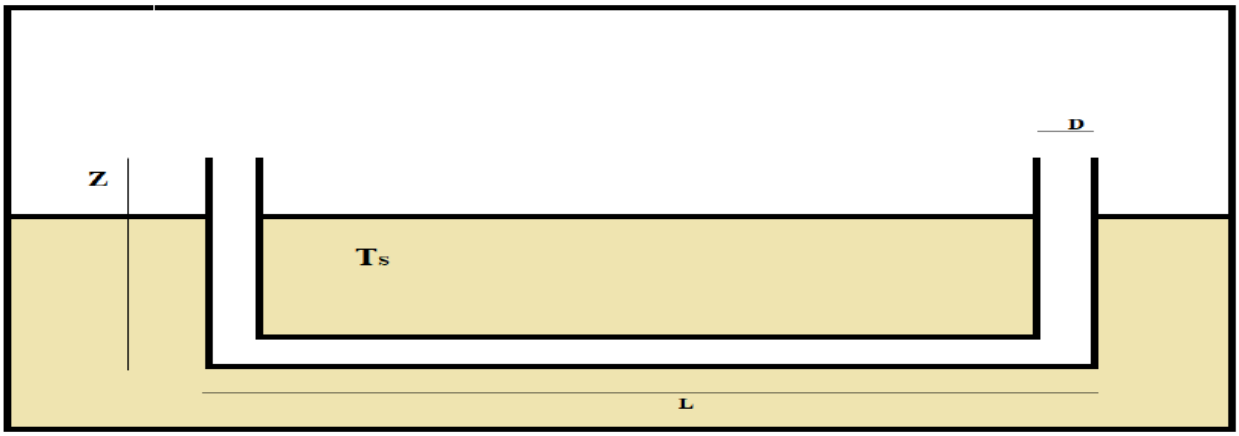

Figure II. 7. Computational Domain

The EAHE as shown in Figure II. 7 consists of a cylindrical tube with an inner diameter of 0.15 m and a length23.42 m buried at a depth of 2.7 m at a temperature of Ts = 26.7 (°C). The velocity of the incoming air changes according to the values (2m/s, 3m/s, 4m/s, 5m/s)

2.8. Physical properties

The operation of an earth air heat exchanger (EAHE) is based on the hot outdoor air being pumped into the underground buried pipe by an adequate fan. The air is cooled by transferring heat to the lower-temperature soil (fig.1). After that, the cooled air is injected into the building. The thermal and physical properties of the air, soil, and pipe used in this simulation are represented in (Table 1).

Table II. 1.Thermalandphysicalpropertiesofair, pipe and soil[53]

Material	Density (kg/m3)	Heat capacity (J/kg.K)	Thermal conductivity (W/m.K)
Air	1.1774	1005.7	0.02624
Soil	2050	1840	0.52
PVC	1380	900	0.16

3. Minitab software presentation

Minitab is a statistical program that allows you to easily enter data and then run a variety of analyses on that data, allowing you to efficiently prepare charts and calculate regression.

Minitab enters data in a manner similar to Excel, and in general, the program requires its users to put in a lot of effort when creating statistics.

The software is a statistical package created in 1972 by a group of researchers at Penn State University[54]. It started out as OMNITAB 80, a statistical analysis program created by the National Institute of Standards and Technology (NIST).

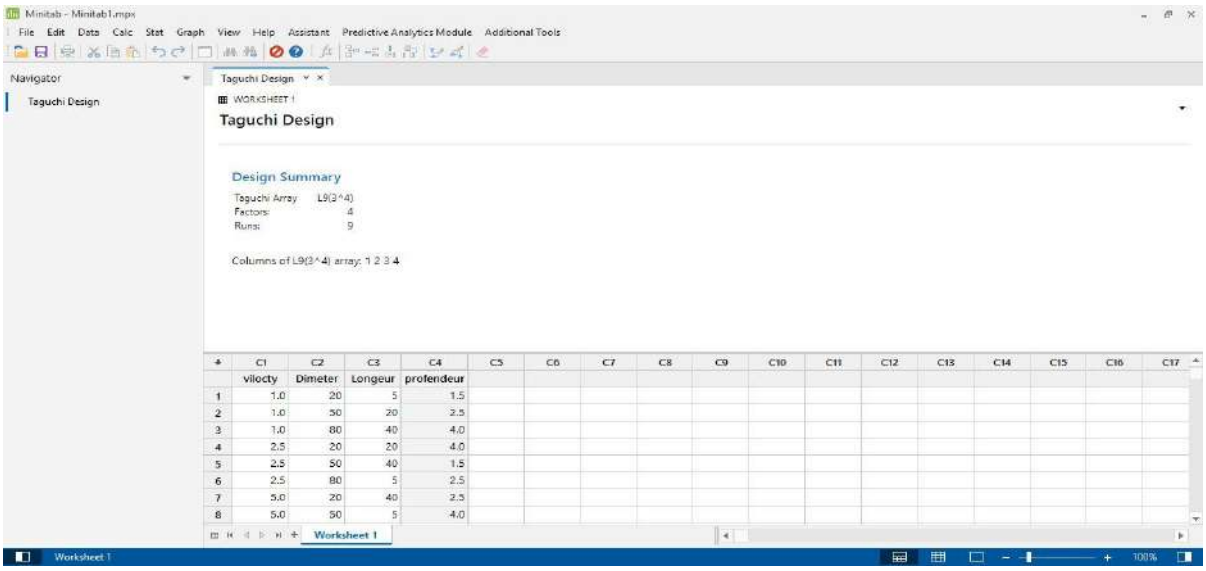

Figure II. 8. Minitab start screen

3.1. Design of experiments

DOE (design of experiments) allows you to simultaneously investigate the effects of input variables (factors) on an output variable (response). These experiments are made up of a series of runs, or tests, in which the input variables are purposefully changed. At the end of each run, data is collected. DOE is used to identify the process conditions and product components that have an impact on quality, and then to determine the factor settings that optimize results. Screening designs, factorial designs, response surface designs, mixture designs, and Taguchi designs are among the five types of designs available in Minitab (also called Taguchi robust designs). The steps in Minitab for creating, analyzing, and visualizing a designed experiment are the same for all types. Minitab provides several analytical and graph tools to help you understand the results after you run the experiment and enter the results. [55]

In this chapter we will study the effect of design parameters such as length, diameter and material of pipe and operating parameters such as velocity and depth on EATHE performance.

3.2. Taguchi Method

The Taguchi method is a statistical technique for laying out the conditions of experiments involving multiple factors to optimize the parameters and improve the system's performance. The method is commonly referred to as factorial design of experiments. A full factorial design will identify all possible combinations for a given set of factors, resulting in a large number of experiments. Taguchi proposed an orthogonal array-based method for studying the entire parameter space (matrix of experiments) with a smaller number of experiments to reduce the number of experiments. With the help of this matrix, one can obtain maximum information from a minimum number of trials, as well as the best level of each parameter for an objective function. For Signal-to-noise (S/N) ratios are used in data analysis to calculate the response of experimental trials. [48]

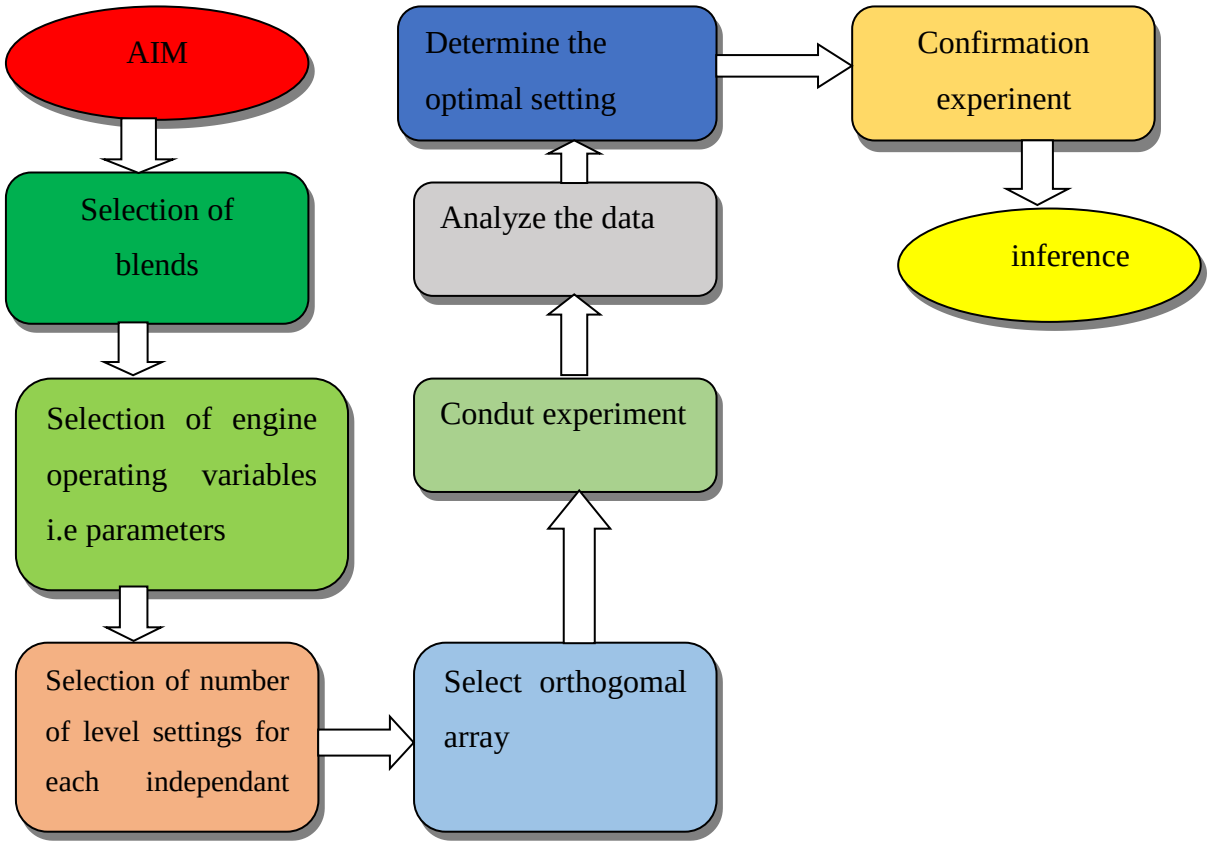

Figure II. 9. Steps in Taguchi method[56].

There are three scenarios: larger-the-better (LTB) for maximization problems, smaller-the-better (STB) for minimization problems, and nominal-thebetter (NTB) for selecting the best characteristic or target value, which is the median of the specified upper and lower acceptable limits, as explained in equations [57]

$$S/NR(LTB) = -10\left[\log\left(\sum\left(\frac{1}{y^2}\right)/n\right)\right] \quad (22)$$

$$S/NR(STB) = -10\left[\log\left(\sum(y^2)/2\right)\right] \quad (23)$$

$$S/NR(NTB) = -10\left[\log\left(\sum(s^2)\right)\right] \quad (24)$$

Where

Y: the number of responses for the given factor level combination

N: denotes the number of responses in the factor level combination.

S: standard deviation of all noise factor responses for the given factor level combination

As shown in Table 3, four parameters at three levels were considered when performing the Taguchi optimisation. The following relation can be used to specify the minimum number of experimental trials to be performed:

$N_{Taguchi} = 1 + nv$ (L-1) [58].

Where $N_{Taguchi}$: denotes the minimum number of experiments or cases to be performed, *nv*: denotes the number of control variables or parameters, and L denotes the number of levels specified nv = 4 and L = 3 for the current study. As a result, 9 computational experiments must be carried out.

The primary objective of this study is to discover the best combination of studied parameters to achieve the maximum effect of EATHE.

Conclusion

In this chapter, we have presented the mathematical formulation allowing the determination of the soil temperature and the air temperature along the air/ground exchanger. and validate our model choose the experimental study by Bansal et al, we also, compared their experimental results with our simulation results in deferent temperature and velocity of the air inlet, at the end we applied Taguchi method to see the effect of factors (Velocity, Diameter, Length and depth) on velocity and temperature.

Chapter III

Results and Discussions

1. Introduction

This chapter presents the different results of the models developed in our study. First, soil temperature profiles are shown to determine the optimum depth of burial for the system.

Then, a validation of the numerical results developed will be carried out with the experimental of Bansal and al [54] then, a CFD study presents the influence of the different thermo-physical and geometric parameters on the thermal behavior of the air-to-ground exchanger. Finally, a result of improvement of the thermal performance of the exchanger has been illustrated.

2. Soil thermal model

2.1. Temperature in soil depth

Figure III.1 illustrates the annual mean variation of soil temperature for three different depths. Table III.1 represents the different thermo physical properties of soil studied (Ouargla region). Note that the average soil temperature increases with depth.

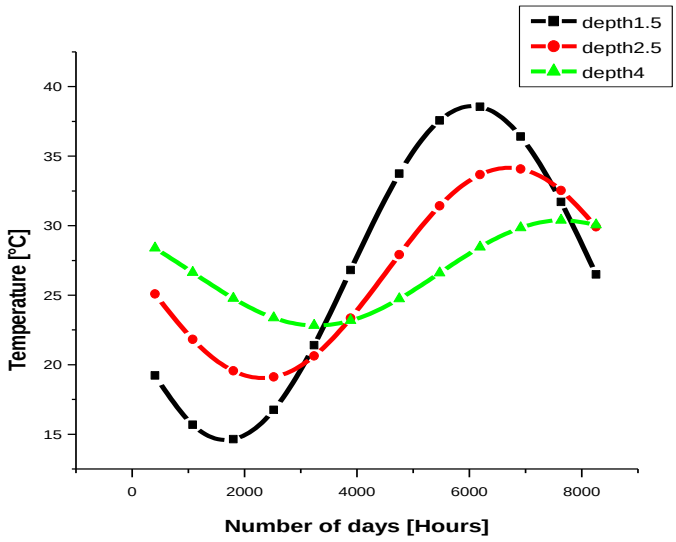

Figure III.1. Hourly change in soil temperature as a function of depth.

The sol's temperature recorded its highest levels in the months of September and October, and recorded its lowest levels in the months of March and April in various depths.

Choosing the best depth plays a very important role in the burial and operation of the air-to-ground exchanger.

3. Model of the air-soil exchanger

The developed CFD model dealing with air temperature along the geothermal air-to-ground heat exchanger has been validated with the experimentation of Bansal et al [59]

Table III.1.Main parameters of the air-soil exchanger used for the validation[59]

parameters taken by Bansal et al	Reference value
Pipe length	23.42 (m)
Pipe diameter	0.15 (m)
Soil density	2050 (kg/m3)
Soil specific heat capacity	1840 (J/Kg. K)
Soil thermal conductivity	0.52 (W/m.°C)
Soil temperature	26.7 (°C)

3.1. Test mesh

Meshing the model using hybrid mesh type by taking different interval size shown in the table III.2

Table III.2. Main parameters of the air-soil exchanger used for the validation

Interval size	Value
Size 01	**0.08**
Size 02	**0.07**
Size 03	**0.06**
Size 04	**0.05**
Size 05	**0.04**
Size 06	**0.03**

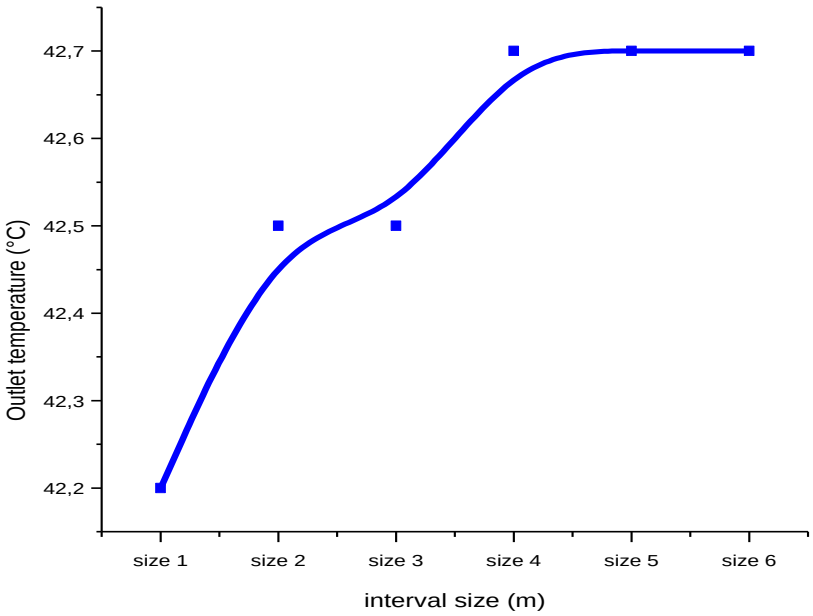

Figure III.2. Outlet temperature for different interval size mesh

From the figure it can be seen that the value of the outlet temperature is stable at a size 4 that corresponds to the value of 0.05 according to the Table III.2.

3.2. Validation results

It is observed in the Table III.3 that there is a good agreement between the simulated results and the experimental results, average relative errors of the order of 7.2 %.are obtained. Therefore, the developed model is validated and can be used for further analysis.

Table III.3. Comparison of experimental and simulated temperature

T	**Air velocity =2m/s**			**Air velocity =3m/s**			**Air velocity=4m/s**			**Air velocity =5m/s**		
	Exp temp	Sim temp	%diff	Exp temp	Sim temp	%dif	Exp temp	Sim temp	%dif	Exp temp	Sim temp	%dif
T_{Inlet}	43.7	43.7	0.00	43.5	43.5	0.00	43.1	43.1	0.00	43.6	43.6	0.00
T_{Outlet}	33.1	29.8	9.97	33.1	30.7	7.25	33.5	31.6	5.74	34.2	32.4	5.44

4. Model optimization

4.1. Choice of factors

Using Taguchi method to improve the heat exchanger, where we chose four factors affecting the performance of the heat exchanger, which are as follows (inlet air velocity, tube length and diameter, and buried depth).

We took 03 different levels for each factor. The factors and levels are shown in Table III.4.

Table III.4. Selected factors and levels

Factor	Parameter	Level		
		L1	L2	L3
A	Velocity m/s	1	2.5	5
B	Diameter cm	20	50	80
C	Length m	5	20	40
D	Depth m	1.5	2.5	4

Table III.5. Taguchi L9 orthogonal array

	Factor A	Factor B	Factor C	Factor D
	Velocity m/s	Diameter cm	Length m	Depth m
01	1.0	20	5	1.5
02	1.0	50	20	2.5
03	1.0	80	40	4.0
04	2.5	20	20	4.0
05	2.5	50	40	1.5
06	2.5	80	5	2.5
07	5.0	20	40	2.5
08	5.0	50	5	4.0
09	5.0	80	20	1.5

5. Simulation results

After we obtained the number of experiments and the characteristics of each experiment, we simulated them using the Gambit and Fluent programs, where we extracted the result of each experiment (temperature and air velocity at the outlet of the heat exchanger). The obtained results are shown in the fifth and sixth columns of Table N° III.6

Table III.6. Outlet temperature of each experiment

Exp	T-outlet
1	38.49
2	39.67
3	36.37
4	29.61
5	39.85
6	47.34
7	29.22
8	47.51
9	46.12

Where we chose July 17 as the hottest day, and we used in the simulation the materials properties and conditions shown in the table N° III.6

Table III.7. Thermal and physical properties of air, pipe and soil [60]

Material	Density (kg/m3)	Heat Capacity (J/kg.K)	Thermal conductivity (W/m.K)
Air	1.1774	1005.7	0.02624
Soil	2050	1840	0.52
PVC	1380	900	0.16

5.1. Effects of the parameters on the outlet temperature

The Figure III.2 show that the greater value of each to two factors, length and depth, the more coldly at the outlet of the heat exchanger, it seen that to the other two factors, the air velocity at the inlet of the heat exchanger and the diameter of the tube have no effect compared with the others are less effective.

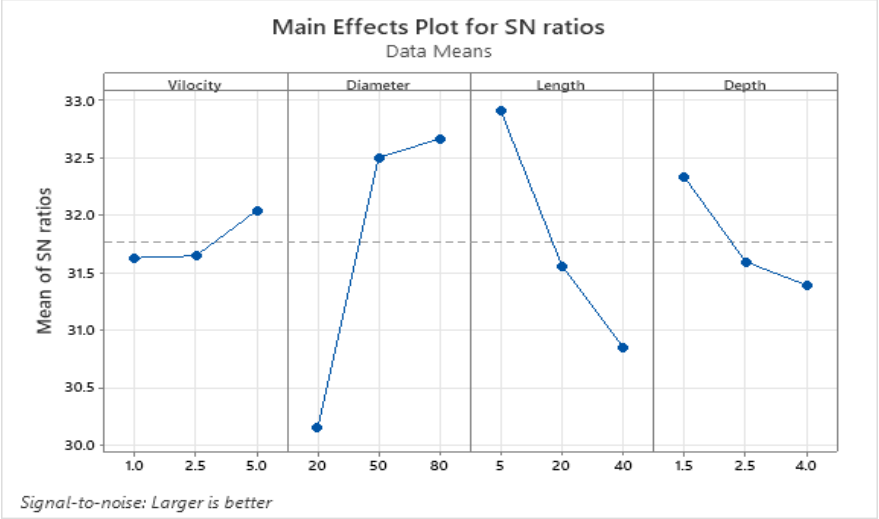

Figure III.3. Effects of the parameters on the outlet temperature

5.2. Optimal configuration

After obtaining the optimal parameter values to obtain a temperature of 28°C at the outlet of the heat exchanger, which is comfortable on the hottest day of the year and the temperature is around 50°C; we simulate the model using Gambit and Flint during a whole year (12 months).

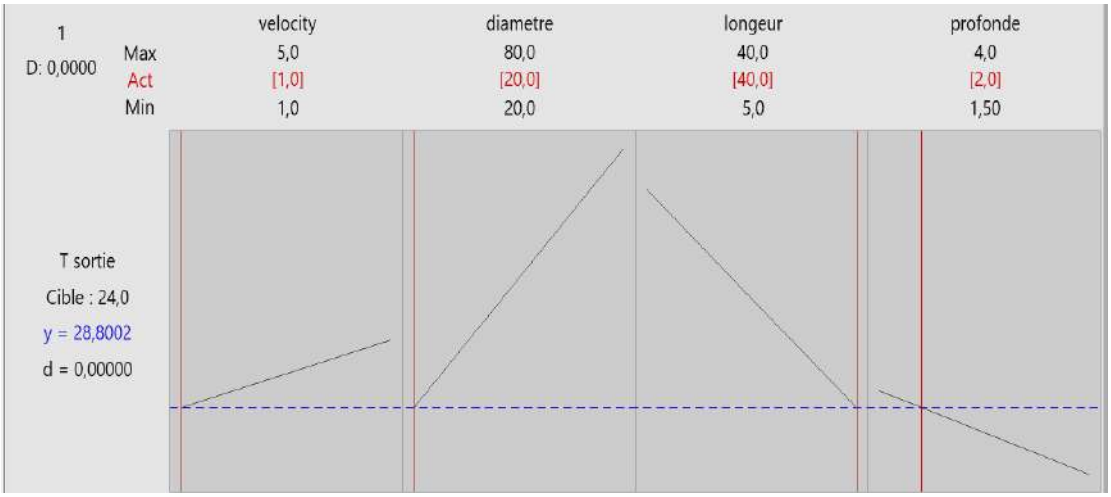

Figure III.4. Optimal configuration

The parameters used in simulation shown in the table III.8

Table III.8. The min max average monthly variation of outdoor temperatures and the average monthly variation of relative humidity and wind speed in the year 2019 [61]

Months	Minimal Temperature (°c)	Maximal Temperature (°c)	Average temperature (°c)	Average relative humidity (%)	Average wind speed (m/s)
January	4	18.4	10.8	40.8	2.9
February	4.9	19.2	12	37.8	3.8
March	9.2	24.2	16.9	33.5	4.0
April	15.5	30.2	23.2	25.9	4.1
May	19	33.3	26.7	25	4.5
June	26.6	42.6	35.3	13.9	4.9
July	28.8	44.5	37.4	13.8	3.6
August	29.7	43.5	36.9	17.8	3.7
September	24	39.1	31.8	27.5	3.6
October	24.2	31	17.2	35.8	2.9
November	9.3	23.3	16.2	37.3	3.1
December	7.1	21.1	13.8	46.7	2.9

6. Results of the developed thermal model of the air-soil exchanger

The obtained results divided into two parts, each section containing the results of 06 months of cooling and 06 months of heating

6.1. Heating performance of the air-ground exchanger

6.1.1. Outlet temperature

The air temperature at the outlet is a key factor in determining the performance of the heat exchanger, so that the higher the temperature at the outlet, the better it is.

The following figures show the temperature at the outlet of the heat exchanger in 06 cold months (October, November, December, January, February, March)

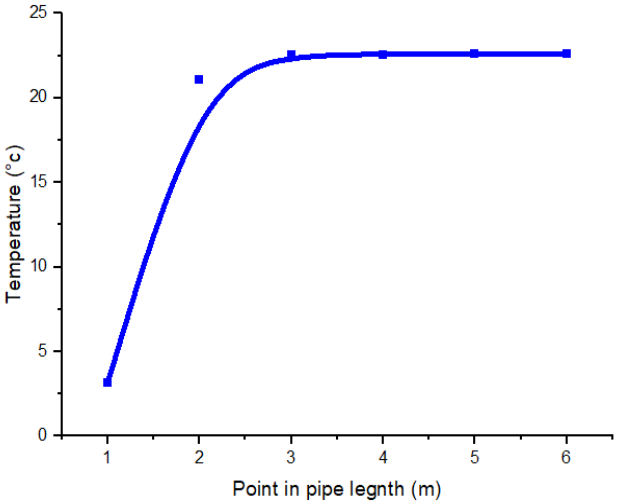

Figure III.5. Outlet temperature in January

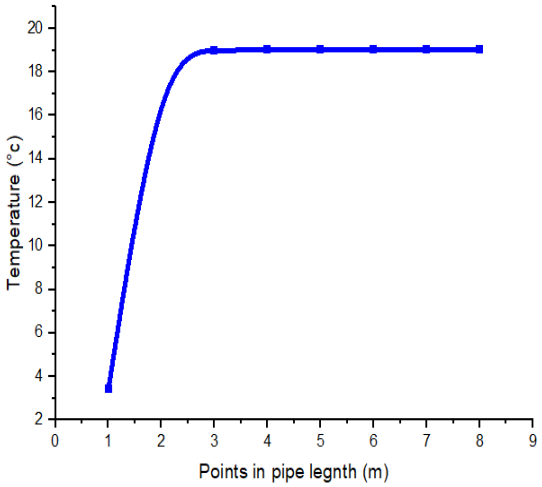

Figure III.6. Outlet temperature in February

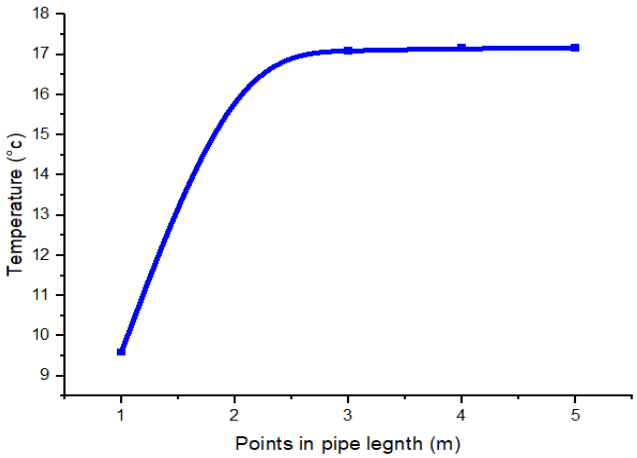

Figure III.7. Outlet temperature in March

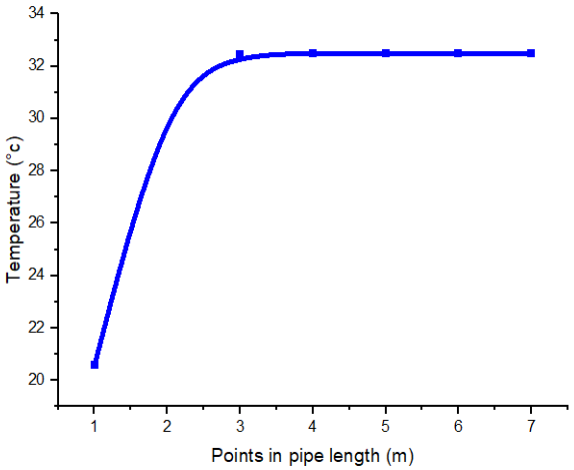

Figure III.8. Outlet temperature in November

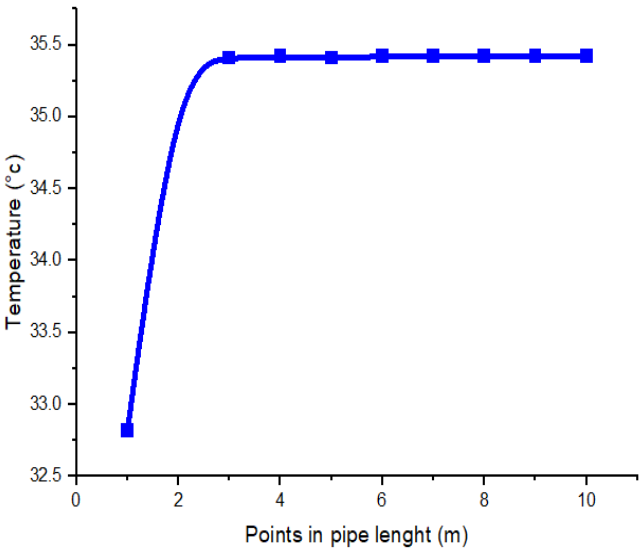

Figure III.9. Outlet temperature in October

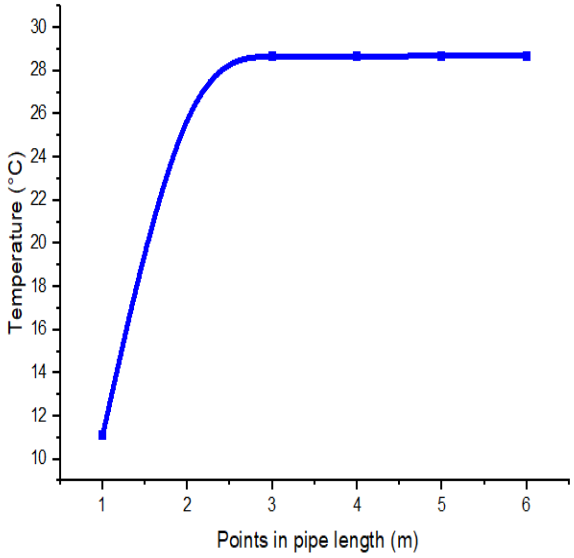

Figure III.10. Outlet temperature in December

Regarding the performance of the exchanger for air heating, the figures reveal that during the cold months (December-March), when the minimum inlet air temperature ranging between 4°C and 9.2°C, the exchanger provides heated air at a temperature level in the range of 17, 35°C.

In principle, it can be said that the air-ground heat exchanger can be considered as a system suitable for heating the air of buildings in a continental climate with mild to cold winters like that of Ouargla

6.1.2. Heating efficiency

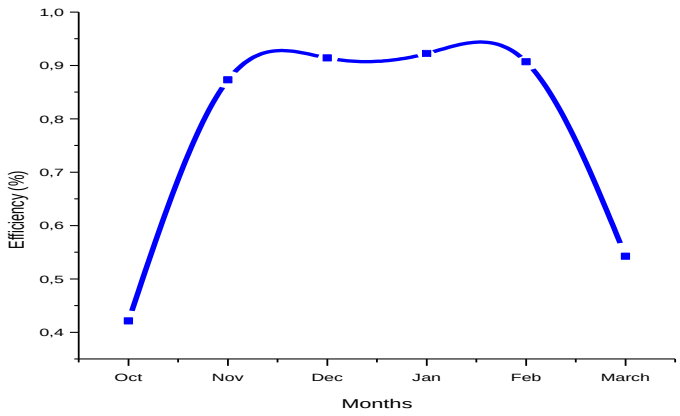

Figure III.11. presents the variation of the thermal efficiency over the months

Figure III.10 presents the variation of the thermal efficiency over the months (Jan, Feb, March, Oct, Nov, Dec) for an air flow speed varying between 2.9 a 4 m/s. it is observed a minimum value of the thermal efficiency of 42%, which is recorded in the month of October when the air temperature at the inlet of the tube is close to ground temperature.

The maximum value of the thermal efficiency is about 92% for an air inlet temperature of 3.15°C. Therefore, the difference in soil and air temperatures plays a very important role in the variation of thermal efficiency.

6.2. Cooling performance of the air-ground exchanger

6.2.1. Outlet temperature

The following figures show the temperature at the outlet of the heat exchanger in 06 hot months (April, May, June, July, August, and September)

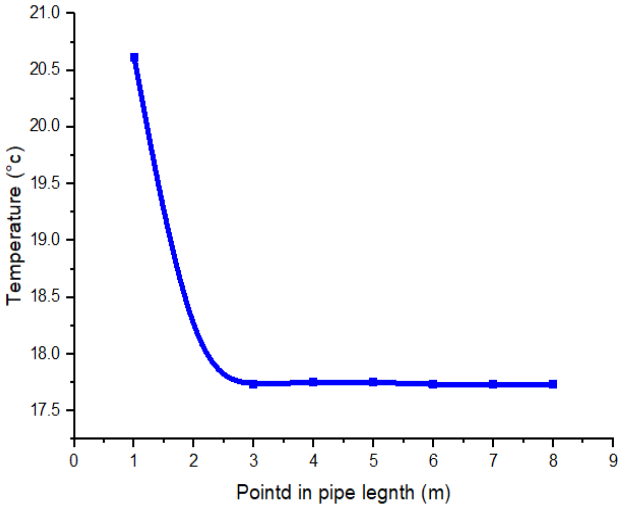

Figure III.12. Outlet temperature in April

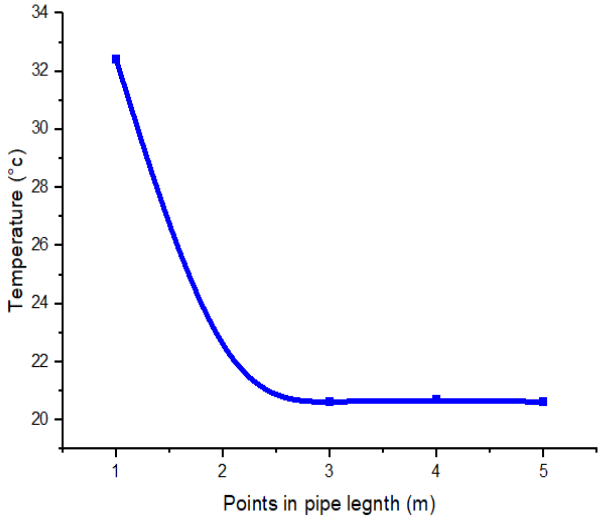

Figure III.13. Outlet temperature in Mai

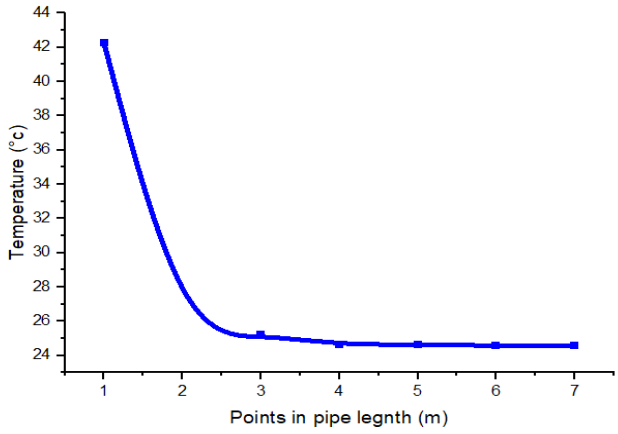

Figure III.14. Outlet temperature in June

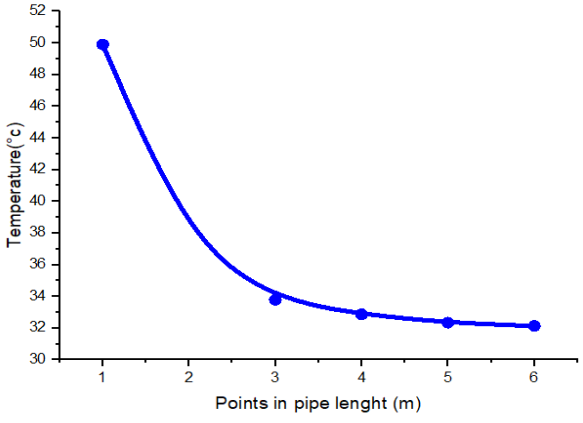

Figure III.15. Outlet temperature in July

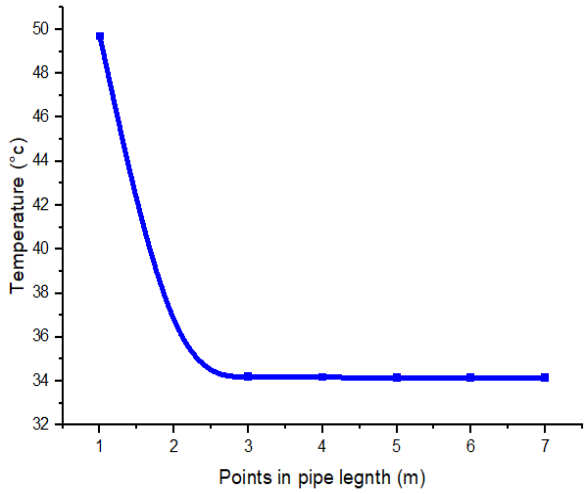

Figure III.16. Outlet temperature in August

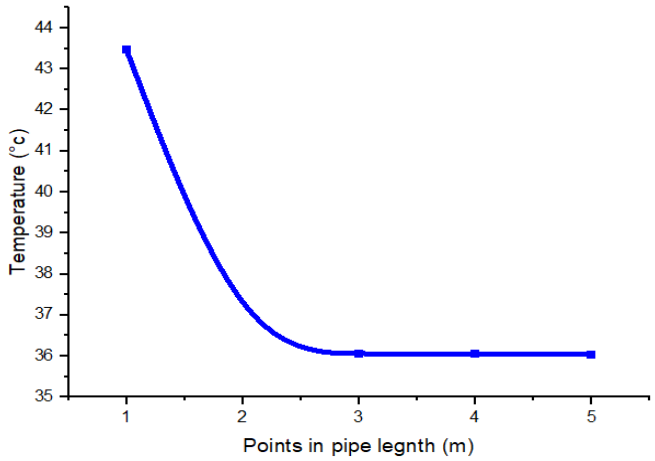

Figure III.17. Outlet temperature in September

Regarding the performance of the exchanger for air cooling, the figures reveal that during the hot months (April -September), when the inlet air temperature ranging between 20°C and 50°C, the exchanger provides cooled air at a temperature level in the range of 19°C.

We note that in the hottest months (July and August), the performance of the heat exchanger is effective, as the air temperature reaches 50 °C, and it cools it down to 32 °C, which is a rather comfortable temperature.

6.2.2. Cooling efficiency

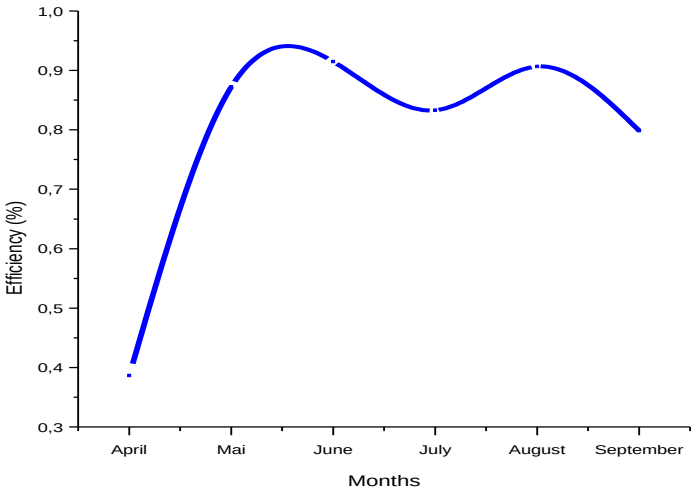

Figure III.18. presents the variation of the thermal efficiency over the months

The variation of the thermal efficiency over the months (April, Mai, June, July, August, September) for an air flow speed varying between 3.6 a 4.9 m/s. it is observed a minimum value of the thermal efficiency of 40%, which is recorded in the month of April when the air temperature at the inlet of the tube is close to ground temperature.

The maximum value of the thermal efficiency is about 91% for an air inlet temperature of 42.24 °C and out 26.08 °C.

6.3. Velocity distribution

To investigate the effect of velocity distribution on heat transfer to air flowing in the pipe.

.

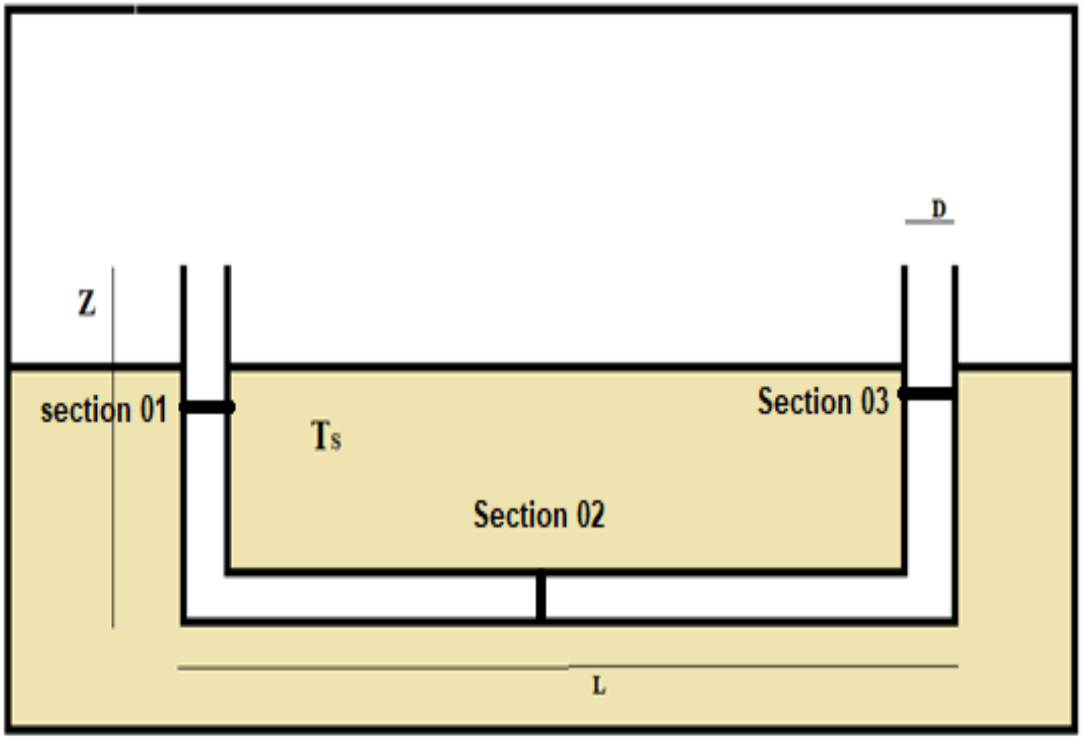

Figure III.19. schematic present the tree sections in the air-ground exchanger model.

The previous figures show yearly velocity distribution in three sections of the pipe. Section 01 in the inlet, section 02 in medium of the pipe, and section 03 near of the outlet as shown in figures III.19.

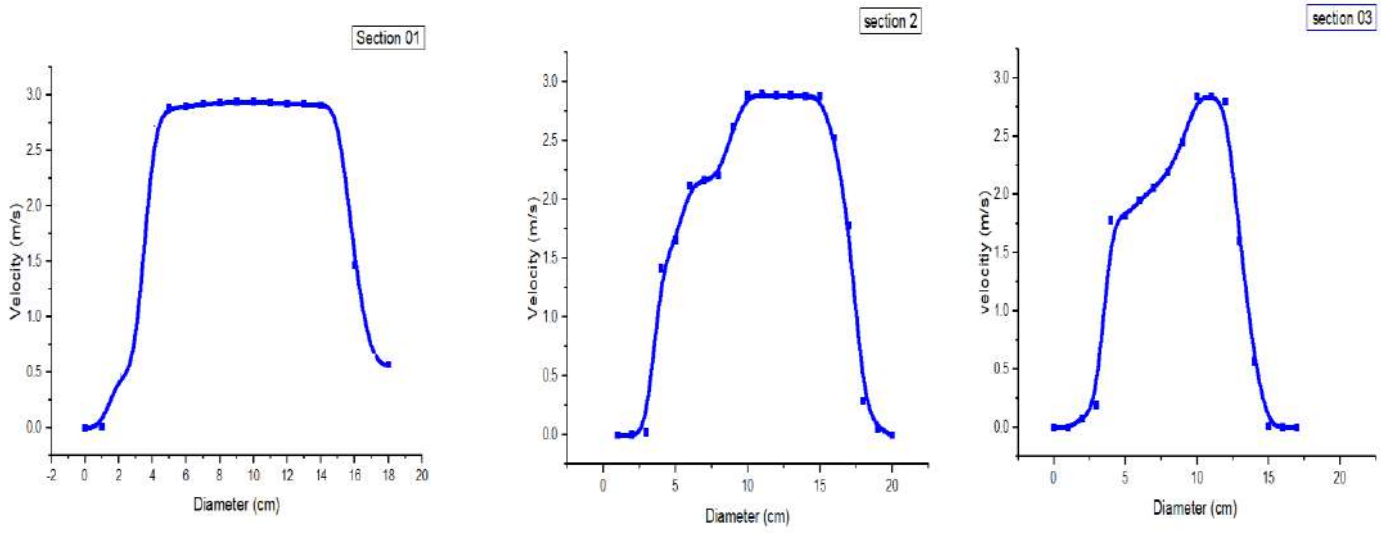

Figure III.20. Velocity distribution over three different sections of the pipe in January

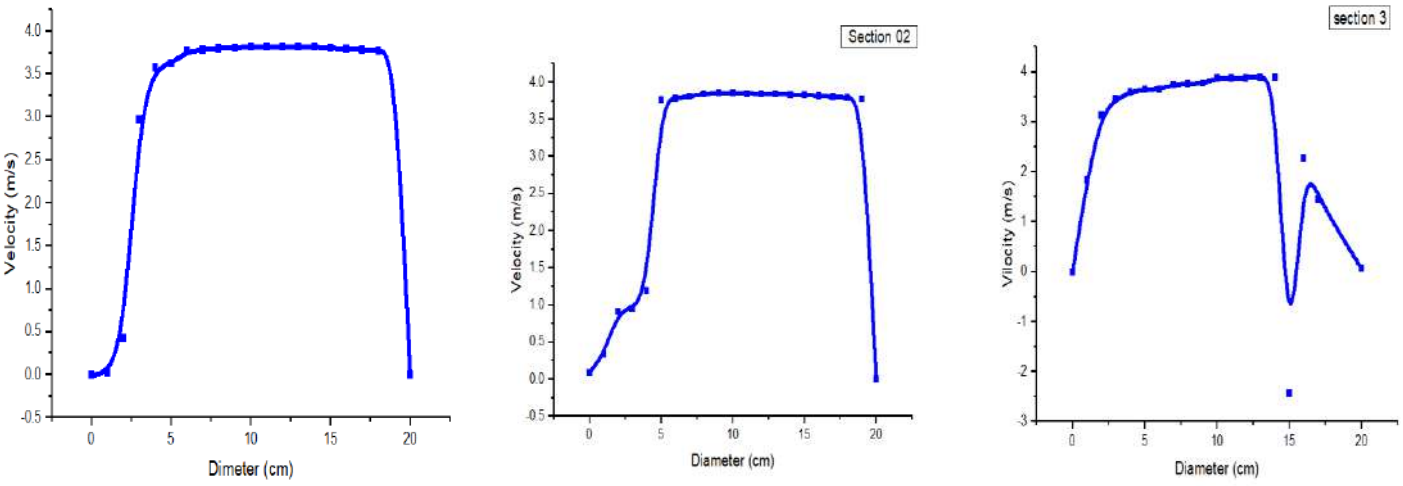

Figure III.21. Velocity distribution over three different sections of the pipe in February

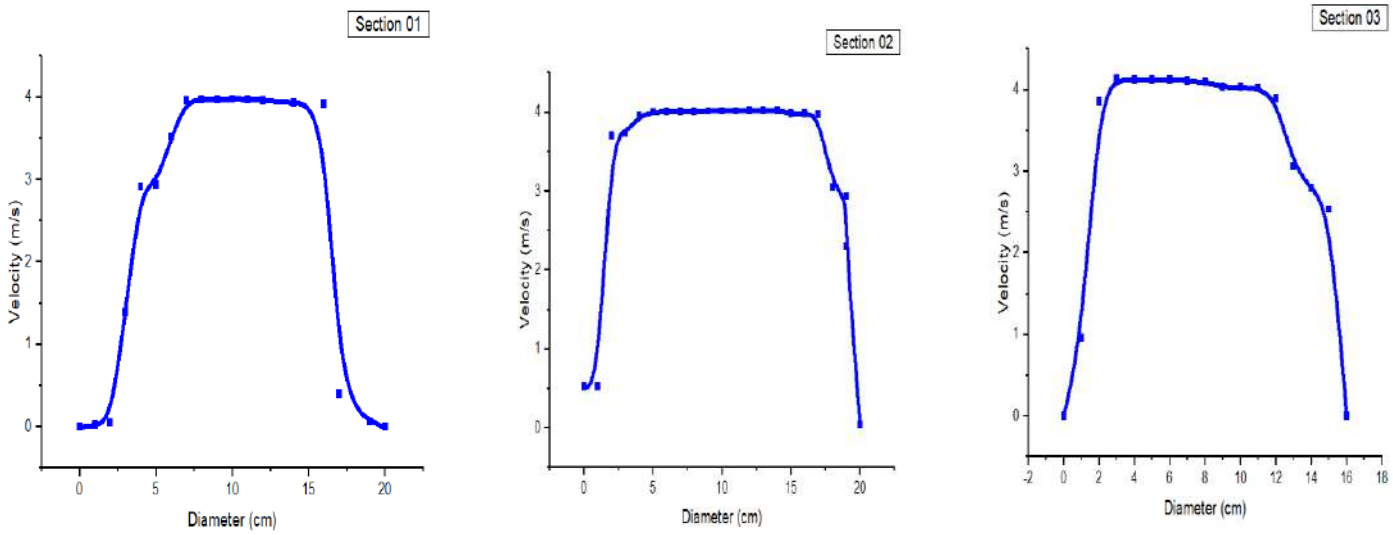

Figure III.22. Velocity distribution over three different sections of the pipe in March

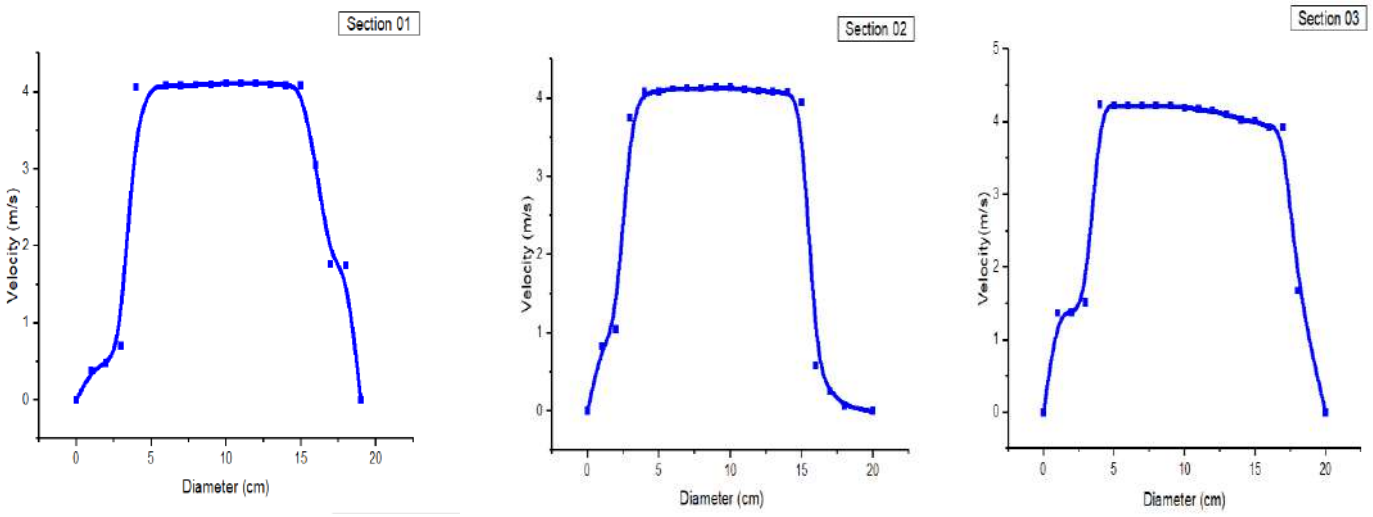

Figure III.23. Velocity distribution over three different sections of the pipe in April

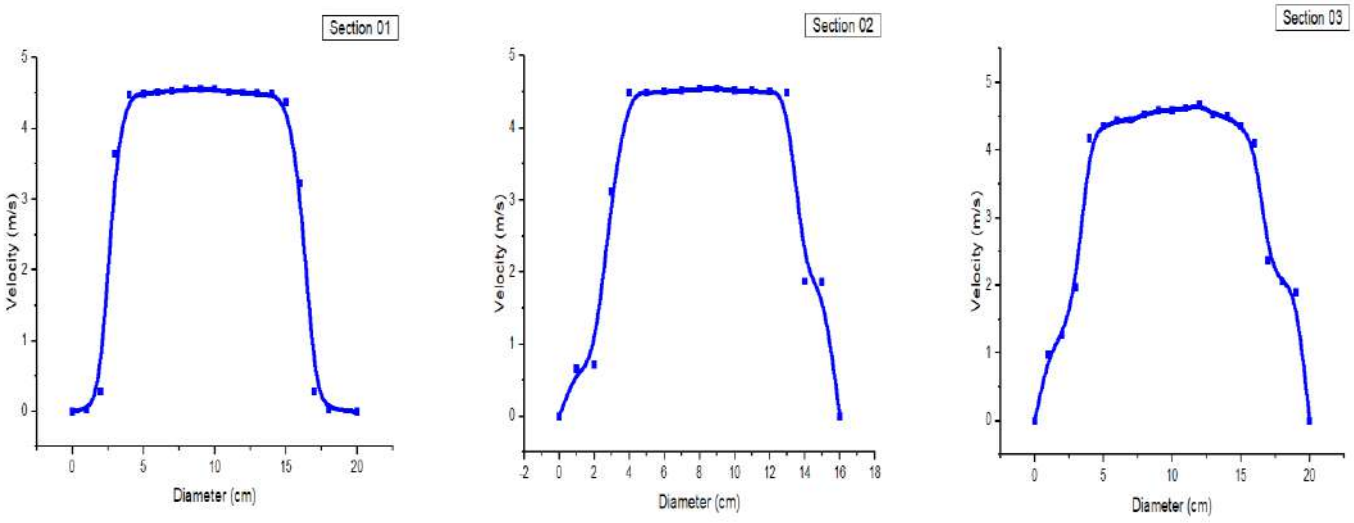

Figure III.24. Velocity distribution over three different sections of the pipe in May

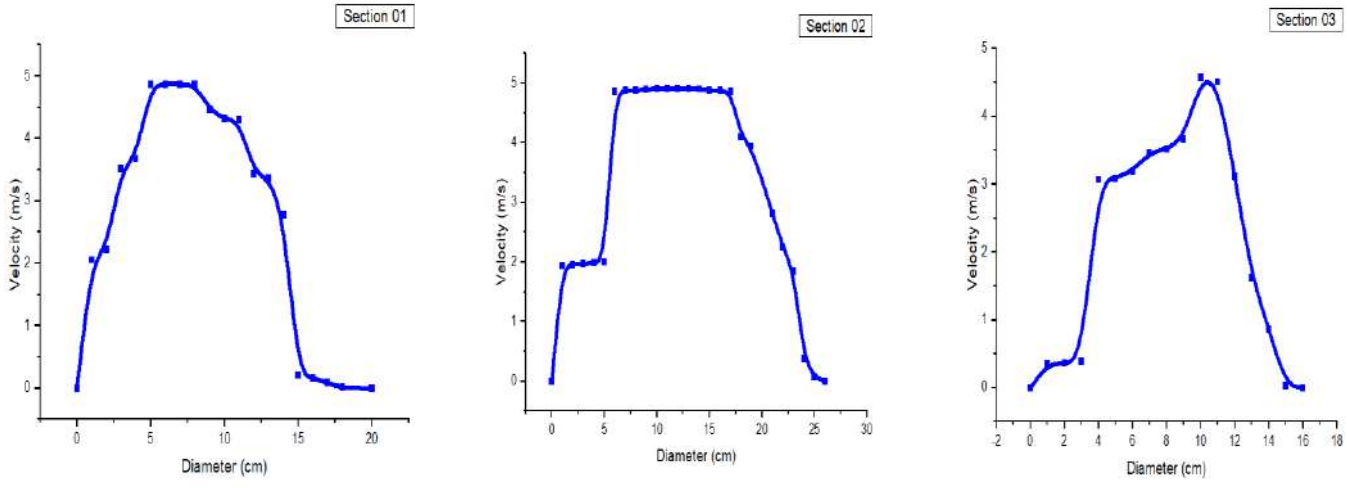

Figure III.25. Velocity distribution over three different sections of the pipe in June

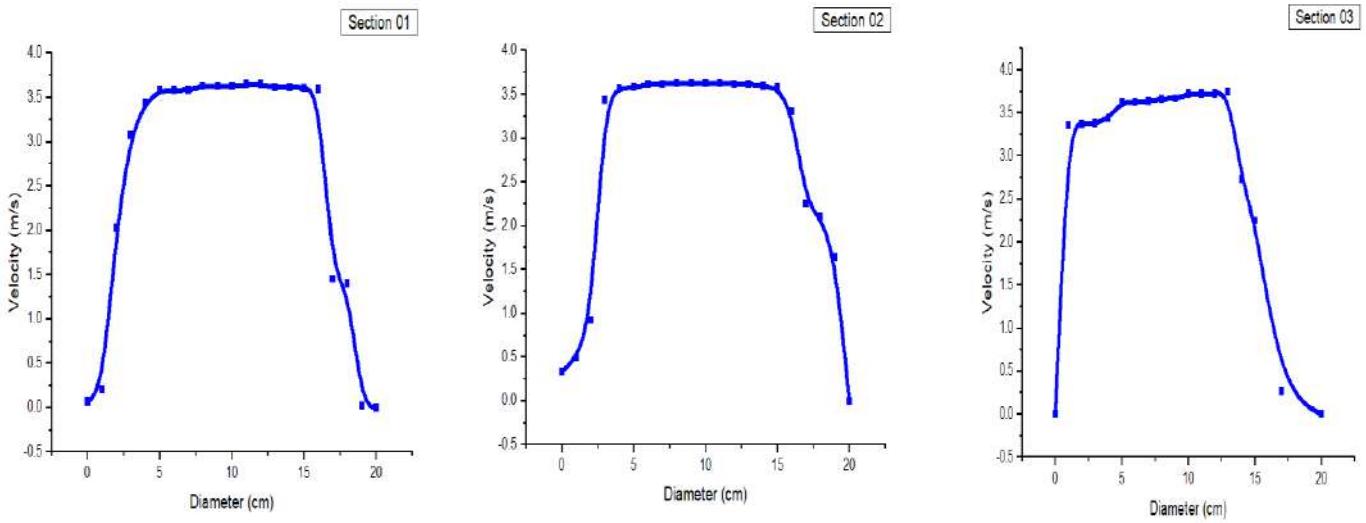

Figure III.26. Velocity distribution over three different sections of the pipe in July

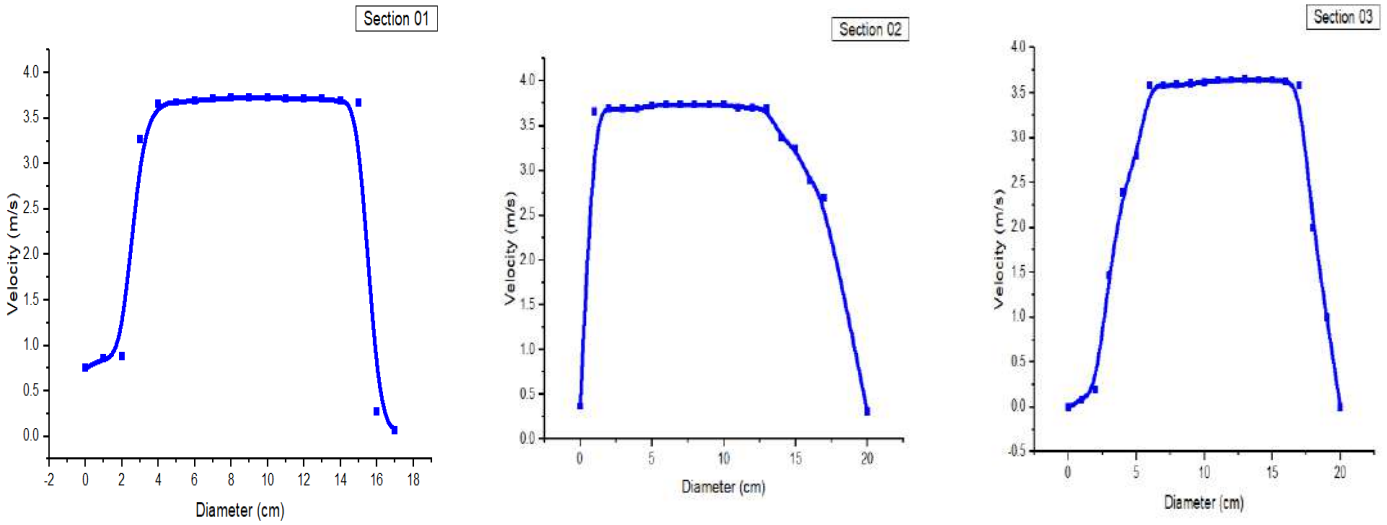

Figure III.27. Velocity distribution over three different sections of the pipe in August

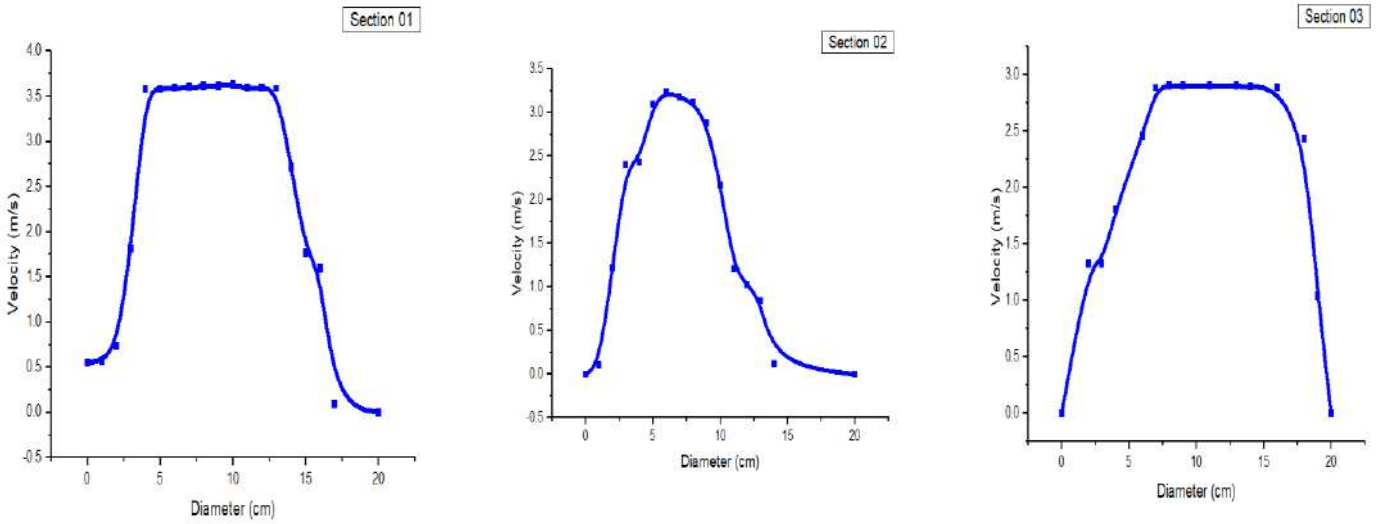

Figure III.28. Velocity distribution over three different sections of the pipe in September

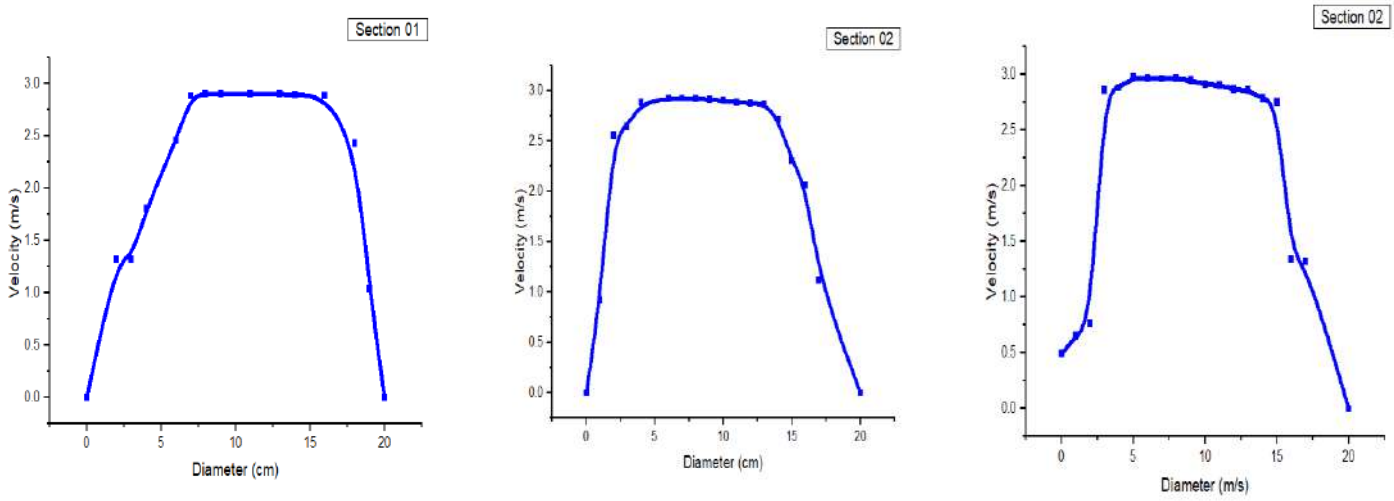

Figure III.29. Velocity distribution over three different sections of the pipe in October

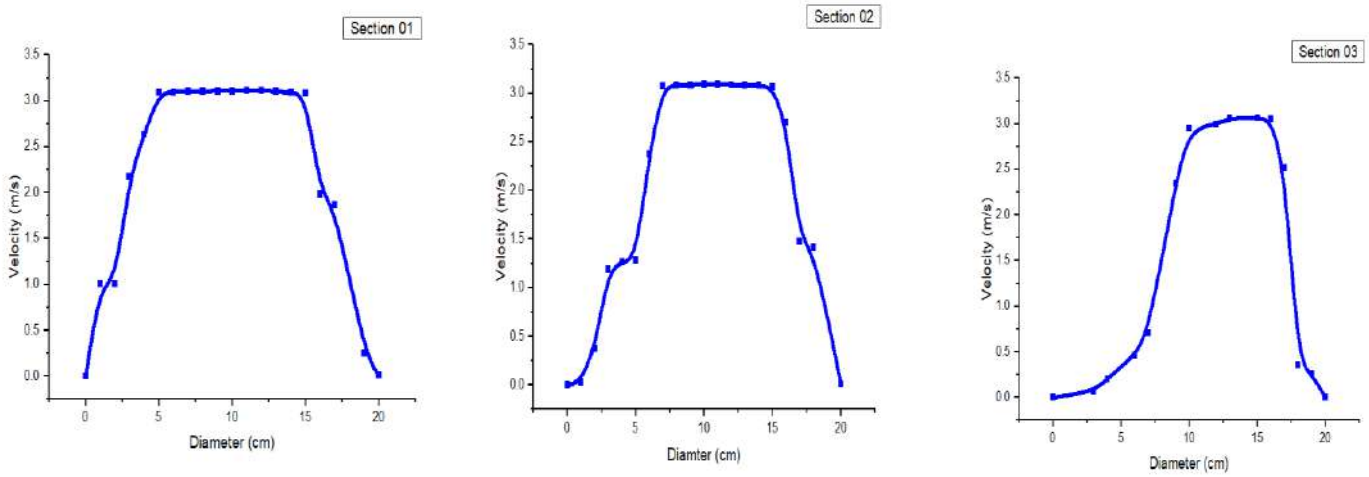

Figure III.30. Velocity distribution over three different sections of the pipe in November

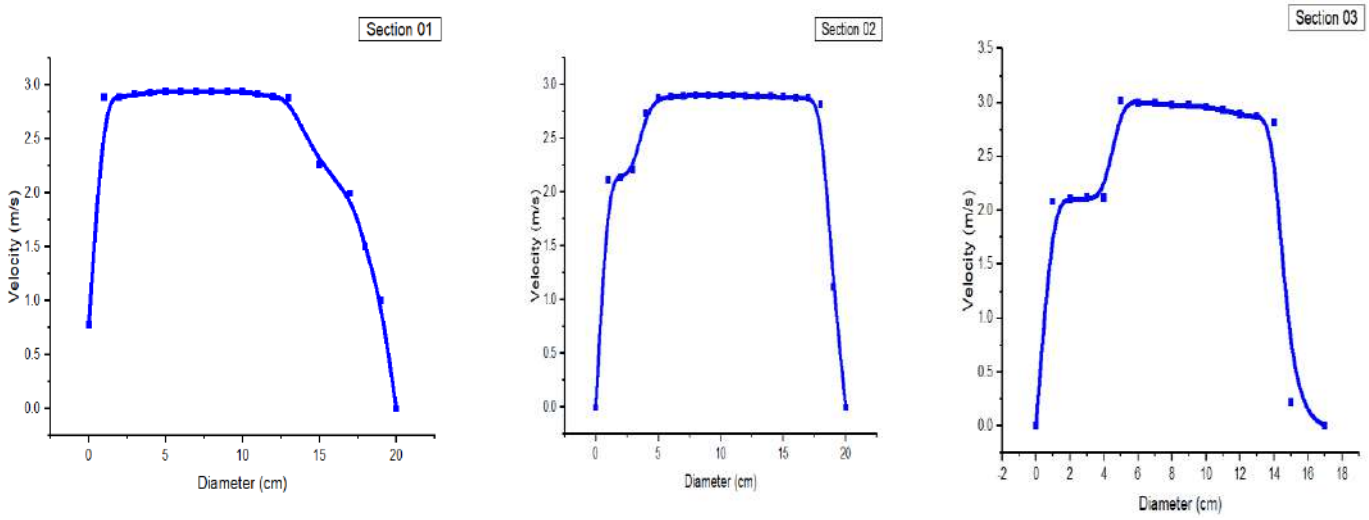

Figure III.31. Velocity distribution over three different sections of the pipe in December

The previous figures show the fluid moving with uniform velocity as it enters the tube. At the tube entrance there is a retardation of the fluid particles next to the wall because of frictional effects. A thin layer then exists in which the fluid velocity builds up from zero at the wall to the core velocity at the edge of the boundary layer. As the fluid moves down the tube the thickness of the boundary layer gradually increases.

The fluid particles next to the wall are heated. There is then a very thin layer in which the temperature decreases from temperature at the wall to the temperature at the center of the pipe.

6.4. Yearly variation of air temperature inside the exchanger

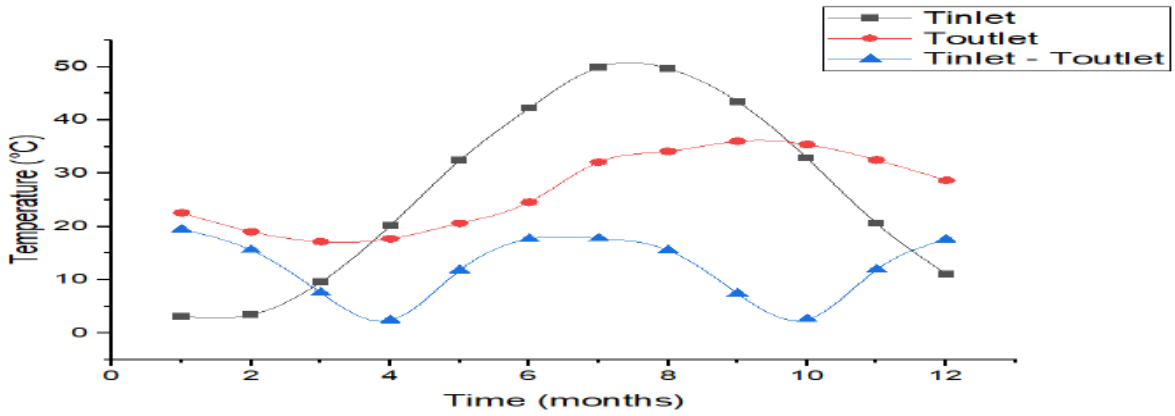

Figure III.32. Monthly temperature profiles over a year of the inlet air, air at the EAHE exit and the temperature difference between both

Figure III.32. show the monthly temperature profiles over a year of the inlet air, the outlet temperature of heat exchanger and the difference between them. It is clear that the performance of the EAHE influenced by the soil temperature and the inlet air temperature because these two parameters change every month. It can also be seen that the maximum temperature difference of air between the inlet and the outlet of the EAHE is around 19.45 °C and 17.77 °C for the months of January and July, respectively, while the minimum temperature difference between the air entering and leaving the EAHE is about 2.44°C and 2.6 °C for the months of April and October, respectively. From these results, it can be concluded that this system is more efficient in the period when the inlet temperature is very cold or very hot.

GENERAL

CONCLUSION

General conclusion

Conclusion

In this thesis we presented a numerical study of the thermal performance of the air-ground exchanger. This study applies Taguchi's design of experiments to see the different relationships between the selected factors and their influence on heat exchanger performance under the climate of Ouargla during the hot season (April-September) and the cold season (October-March).

First, we modeled the soil equation and built a program in Python language to calculate the earth's temperature throughout the year and at varying depths, where the results showed that the deeper we go, the higher the earth's temperature until it stabilizes and becomes stable.

This study revealed that the most influential parameters on the thermal performance of the exchanger are the length and diameter of the tube, its depth of burial and the speed of the air entering, A complete parametric study on these four parameters has was carried out on an air-ground exchanger found in literature and already validated by experimentation (Bansal et al) in order to achieve the optimal configuration of the air-to-ground exchanger model.
Established that:

- Increasing the length of the tube increases the temperature of the outlet air.
- Increasing the burial depth considerably increases the outlet air temperature.
- The investment cost, which increases with depth, must be taken into consideration when dimensioning.
- The increase in air speed leads to a decrease at outlet air temperature.

After obtaining the optimal four factors, building a model based on these factors, and simulating it CFD over a year, the results were as follows:

The system can work efficiently and provide a comfortable temperature during the two seasons, summer and winter, especially when the temperature is very high or very low.

BIBLIOGRAPHIC REFERENC

1. Amri, F., *The relationship amongst energy consumption (renewable and non-renewable), and GDP in Algeria.* Renewable and Sustainable Energy Reviews, 2017. **76**: p. 62-71.

2. Nouri, G., Y. Noorollahi, and H. Yousefi, *Designing and optimization of solar assisted ground source heat pump system to supply heating, cooling and hot water demands.* Geothermics, 2019. **82**: p. 212-231.

3. Ghedamsi, R., et al., *Modeling and forecasting energy consumption for residential buildings in Algeria using bottom-up approach.* Energy and Buildings, 2016. **121**: p. 309-317.

4. Noureddine, A. and S.M.A. Ahmed, *Analyse numérique des performances thermiques d'un système d'échange de chaleur Terre-Air fonctionnanten climat chaud*, in *DEPARTEMENT DE GENIE MECANIQUE*. 2020/2021, Université Echahid Hamma Lakhdar d'El-Oued. p.1.

5. Benhammou, M. and B. Draoui, *Modélisation de la température en profondeur du sol pour la région d'Adrar-Effet de la nature du sol.* Journal of Renewable Energies, 2011. **14**(2): p. 219–228-219–228.

6. Singh, R., et al., *Recent advancements in earth air tunnel heat exchanger (EATHE) system for indoor thermal comfort application: A review.* Renewable and Sustainable Energy Reviews, 2018. **82**: p. 2162-2185.

7. BELATRACHE, D. and S. BENTOUBA, *Contribution à l'optimisation et l'amélioration de l'isolation d'une habitation utilisant une source renouvelable dans les zones arides*. 2018, Université Ahmed Draia-ADRAR.

8. Barakat, S., et al., *Augmentation of gas turbine performance using integrated EAHE and Fogging Inlet Air Cooling System.* Energy, 2019. **189**: p. 116133.

9. Gao, X., Y. Xiao, and P. Gao, *Thermal potential improvement of an earth-air heat exchanger (EAHE) by employing backfilling for deep underground emergency ventilation.* Energy, 2022. **250**: p. 123783.

10. Belloufi, Y., et al., *Transient assessment of an earth air heat exchanger in warm climatic conditions.* Geothermics, 2022. **104**: p. 102442.

11. Li, H., et al., *Experimental investigation on the cooling performance of an Earth to Air Heat Exchanger (EAHE) equipped with an irrigation system to adjust soil moisture.* Energy and Buildings, 2019. **196**: p. 280-292.

12. Hegazi, A., O. Abdelrehim, and A. Khater, *Parametric optimization of earth-air heat exchangers (EAHEs) for central air conditioning.* International Journal of Refrigeration, 2021. **129**: p. 278-289.

13. Rouag, A., A. Benchabane, and C.-E. Mehdid, *Thermal design of Earth-to-Air Heat Exchanger. Part I a new transient semi-analytical model for determining soil temperature.* Journal of cleaner production, 2018. **182**: p. 538-544.

14. Calautit, J.K., et al., *Development of a natural ventilation windcatcher with passive heat recovery wheel for mild-cold climates: CFD and experimental analysis.* Renewable Energy, 2020. **160**: p. 465-482.

15. Zaki, A., P. Richards, and R. Sharma, *Analysis of airflow inside a two-sided wind catcher building.* Journal of Wind Engineering and Industrial Aerodynamics, 2019. **190**: p. 71-82.

16. Sadeghi, M., et al., *Comfort cooling by wind towers in the Australian residential context–Experimental wind tunnel study of comfort.* Journal of Wind Engineering and Industrial Aerodynamics, 2020. **196**: p. 104014.

17. Goudarzi, N., et al., *Airflow and thermal comfort evaluation of a room with different outlet opening sizes and elevations ventilated by a two-sided wind catcher.* Journal of Building Engineering, 2021. **37**: p. 102112.

18. Ganesh, G.A., et al., *Numerical simulation for energy consumption and thermal comfort in a naturally ventilated indoor environment under different orientations of inlet diffuser.* Building and Environment, 2022. **217**: p. 109071.

19. Miri, A., et al., *In-situ measurements of indoor dust deposition in Sistan region, Iran–the effect of windcatcher orientation.* Building and Environment, 2022: p. 109162.

20. Mohamadabadi, H.D., et al., *Numerical and experimental performance analysis of a four-sided wind tower adjoining parlor and courtyard at different wind incident angles.* Energy and Buildings, 2018. **172**: p. 525-536.

21. Alwetaishi, M. and M. Gadi, *New and innovative wind catcher designs to improve indoor air quality in buildings.* Energy and Built Environment, 2021. **2**(4): p. 337-344.

22. Pakari, A. and S. Ghani, *Airflow assessment in a naturally ventilated greenhouse equipped with wind towers: Numerical simulation and wind tunnel experiments.* Energy and Buildings, 2019. **199**: p. 1-11.

23. Yang, L., et al., *Ventilation effect on different position of classrooms in "line" type teaching building.* Journal of Cleaner Production, 2019. **209**: p. 886-902.

24. Jafari, S. and V. Kalantar, *Numerical simulation of natural ventilation with passive cooling by diagonal solar chimneys and windcatcher and water spray system in a hot and dry climate.* Energy and Buildings, 2022. **256**: p. 111714.

25. Jahangir, M.H. and S. Labbafi, *Optimization of ground source heat pump system along with energy storage tank armed with phase change materials to improve the microalgae open culture system performance.* Journal of Energy Storage, 2022. **51**: p. 104436.

26. Biglarian, H. and S. Abdollahi, *Utilization of on-grid photovoltaic panels to offset electricity consumption of a residential ground source heat pump.* Energy, 2022. **243**: p. 122770.

27. Hu, R., et al., *Field study on cooling performance of a heat recovery ground source heat pump system coupled with thermally activated building systems (TABSs).* Energy Conversion and Management, 2022. **262**: p. 115678.

28. Luo, L., et al., *Energy efficiency and environmental assessment of an integrated ground source heat pump and anaerobic digestion system.* Journal of Building Engineering, 2022. **54**: p. 104613.

29. Nordgård-Hansen, E., et al., *Case study on optimal design and operation of detached house energy system: Solar, battery, and ground source heat pump.* Applied Energy, 2022. **308**: p. 118370.

30. Liu, Z., et al., *Performance and feasibility study of hybrid ground source heat pump system assisted with cooling tower for one office building based on one Shanghai case.* Energy, 2019. **173**: p. 28-37.

31. Lee, M., et al., *Performance improvement of solar-assisted ground-source heat pumps with parallelly connected heat sources in heating-dominated areas.* Energy, 2022. **240**: p. 122807.

32. Shimada, Y., et al., *Subsurface utilization as a heat sink for large-scale ground source heat pump: Case study in Bangkok, Thailand.* Renewable Energy, 2021. **180**: p. 966-979.

33. Violante, A.C., et al., *Comparative life cycle assessment of the ground source heat pump vs air source heat pump.* Renewable Energy, 2022. **188**: p. 1029-1037.

34. Naili, N. and S. Kooli, *Solar-assisted ground source heat pump system operated in heating mode: A case study in Tunisia.* Renewable and Sustainable Energy Reviews, 2021. **145**: p. 111144.

35. Zhou, K., et al., *Thermal and economic performance of horizontal ground source heat pump systems with different flowrate control methods.* Journal of Building Engineering, 2022. **53**: p. 104554.

36. Amri, F., *The relationship amongst energy consumption (renewable and non-renewable), and GDP in Algeria.* Renewable and Sustainable Energy Reviews, 2017. **76**: p. 62-71.

37. Nouri, G., Y. Noorollahi, and H. Yousefi, *Designing and optimization of solar assisted ground source heat pump system to supply heating, cooling and hot water demands.* Geothermics, 2019. **82**: p. 212-231.

38. Ghedamsi, R., et al., *Modeling and forecasting energy consumption for residential buildings in Algeria using bottom-up approach.* Energy and Buildings, 2016. **121**: p. 309-317.

39. Noureddine, A. and S.M.A. Ahmed, *Analyse numérique des performances thermiques d'un système*

d'échange de chaleur Terre-Air fonctionnanten climat chaud, in *DEPARTEMENT DE GENIE MECANIQUE*. 2020/2021, Université Echahid Hamma Lakhdar d'El-Oued. p. 1.
40. Singh, R., et al., *Recent advancements in earth air tunnel heat exchanger (EATHE) system for indoor thermal comfort application: A review.* Renewable and Sustainable Energy Reviews, 2018. **82**: p. 2162-2185.
41. BELATRACHE, D. and S. BENTOUBA, *Contribution à l'optimisation et l'amélioration de l'isolation d'une habitation utilisant une source renouvelable dans les zones arides*. 2018, Université Ahmed Draia-ADRAR.
42. Barakat, S., et al., *Augmentation of gas turbine performance using integrated EAHE and Fogging Inlet Air Cooling System.* Energy, 2019. **189**: p. 116133.
43. Gao, X., Y. Xiao, and P. Gao, *Thermal potential improvement of an earth-air heat exchanger (EAHE) by employing backfilling for deep underground emergency ventilation.* Energy, 2022. **250**: p. 123783.
44. Belloufi, Y., et al., *Transient assessment of an earth air heat exchanger in warm climatic conditions.* Geothermics, 2022. **104**: p. 102442.
45. Hegazi, A., O. Abdelrehim, and A. Khater, *Parametric optimization of earth-air heat exchangers (EAHEs) for central air conditioning.* International Journal of Refrigeration, 2021. **129**: p. 278-289.
46. Rouag, A., A. Benchabane, and C.-E. Mehdid, *Thermal design of Earth-to-Air Heat Exchanger. Part I a new transient semi-analytical model for determining soil temperature.* Journal of cleaner production, 2018. **182**: p. 538-544.
47. Zaki, A., P. Richards, and R. Sharma, *Analysis of airflow inside a two-sided wind catcher building.* Journal of Wind Engineering and Industrial Aerodynamics, 2019. **190**: p. 71-82.
48. Sadeghi, M., et al., *Comfort cooling by wind towers in the Australian residential context–Experimental wind tunnel study of comfort.* Journal of Wind Engineering and Industrial Aerodynamics, 2020. **196**: p. 104014.
49. Goudarzi, N., et al., *Airflow and thermal comfort evaluation of a room with different outlet opening sizes and elevations ventilated by a two-sided wind catcher.* Journal of Building Engineering, 2021. **37**: p. 102112.
50. Ganesh, G.A., et al., *Numerical simulation for energy consumption and thermal comfort in a naturally ventilated indoor environment under different orientations of inlet diffuser.* Building and Environment, 2022. **217**: p. 109071.
51. Miri, A., et al., *In-situ measurements of indoor dust deposition in Sistan region, Iran–the effect of windcatcher orientation.* Building and Environment, 2022: p. 109162.
52. Mohamadabadi, H.D., et al., *Numerical and experimental performance analysis of a four-sided wind tower adjoining parlor and courtyard at different wind incident angles.* Energy and Buildings, 2018. **172**: p. 525-536.
53. Alwetaishi, M. and M. Gadi, *New and innovative wind catcher designs to improve indoor air quality in buildings.* Energy and Built Environment, 2021. **2**(4): p. 337-344.
54. Pakari, A. and S. Ghani, *Airflow assessment in a naturally ventilated greenhouse equipped with wind towers: Numerical simulation and wind tunnel experiments.* Energy and Buildings, 2019. **199**: p. 1-11.
55. Yang, L., et al., *Ventilation effect on different position of classrooms in "line" type teaching building.* Journal of Cleaner Production, 2019. **209**: p. 886-902.
56. Jafari, S. and V. Kalantar, *Numerical simulation of natural ventilation with passive cooling by diagonal solar chimneys and windcatcher and water spray system in a hot and dry climate.* Energy and Buildings, 2022. **256**: p. 111714.

57. Jahangir, M.H. and S. Labbafi, *Optimization of ground source heat pump system along with energy storage tank armed with phase change materials to improve the microalgae open culture system performance.* Journal of Energy Storage, 2022. **51**: p. 104436.
58. Biglarian, H. and S. Abdollahi, *Utilization of on-grid photovoltaic panels to offset electricity consumption of a residential ground source heat pump.* Energy, 2022. **243**: p. 122770.
59. Hu, R., et al., *Field study on cooling performance of a heat recovery ground source heat pump system coupled with thermally activated building systems (TABSs).* Energy Conversion and Management, 2022. **262**: p. 115678.
60. Luo, L., et al., *Energy efficiency and environmental assessment of an integrated ground source heat pump and anaerobic digestion system.* Journal of Building Engineering, 2022. **54**: p. 104613.
61. Nordgård-Hansen, E., et al., *Case study on optimal design and operation of detached house energy system: Solar, battery, and ground source heat pump.* Applied Energy, 2022. **308**: p. 118370.
62. Liu, Z., et al., *Performance and feasibility study of hybrid ground source heat pump system assisted with cooling tower for one office building based on one Shanghai case.* Energy, 2019. **173**: p. 28-37.

Annex

Annex: Metrological Data of Ouargla (2011-2021)

2011	T	TM	Tm	H	PP	V
JANUARY	12.4	20.2	5.5	58.3	0	9.3
FEBRUARY	13.2	20.6	5.8	48.7	0	13.7
MARCH	17.3	23.9	9.5	47.2	18.55	17.6
APRIL	23.7	30.9	15	37.5	31.42	17.8
MAY	27	34.1	18.9	35.7	0	17.6
JUNE	31.8	38.5	23.5	33.6	0	17.3
JULY	36.7	44	28	27.7	0	15.6
AUGUST	35.3	42.3	26.4	29.3	0	14.7
SEPTEMBER	33.1	40.4	25.4	30.9	0	16.1
OCTOBER	22.3	29.2	15.2	53.5	5.08	11
NOVEMBER	17.1	24.4	10.1	55.8	0	12
DECEMBER	12	19.7	5.4	67.5	0	9.1
Moy	23.492	30.68333333	15.725	43.80833	4.5875	14.31667
2012	**T**	**TM**	**Tm**	**H**	**PP**	**V**
JANUARY	10.8	18	3.9	62.5	16.01	13.2
FEBRUARY	10.6	17.3	3.7	55.9	6.1	14.8
MARCH	17.2	24.5	9.3	49.5	1.53	12
APRIL	23.3	30.4	14.8	37.5	4.06	17.4
MAY	28.7	35.5	19.9	29.4	0	17.9
JUNE	36.6	43.3	27.7	25.2	0	13.5
JULY	38	44.9	28.7	22.8	0	12.5
AUGUST	35.8	43.1	27.2	23.9	0	13.4
SEPTEMBER	31	38.1	22.6	28.5	25.91	12.3
OCTOBER	26	33.5	18.5	35.5	1.02	12.8
NOVEMBER	19.3	26.3	12.3	50.5	0	10.9
DECEMBER	11.6	20.1	3.8	55.6	0	6.7
Moy	24.075	31.25	16.03333	39.73333	4.5525	13.11667
2013	**T**	**TM**	**Tm**	**H**	**PP**	**V**
JANUARY	13.1	20.2	5.8	51.7	0	12.3
FEBRUARY	13.3	21.3	5.8	46.4	0	14.6
MARCH	20.7	28.5	12.2	45	0	14.9
APRIL	23.7	31	15.8	34.8	6.35	19.8
MAY	28	35.4	19.2	20.4	0	15.7
JUNE	32.2	39.8	23.3	18.1	0	16.9
JULY	36.8	34.5	28	16	0	14.4
AUGUST	33.8	40.1	26.6	21.2	2.03	14.7
SEPTEMBER	31.3	37.9	23.8	26	0	15.2
OCTOBER	26.8	34.6	19.1	26.3	0	8.8
NOVEMBER	16.6	23.3	10	41.9	5.08	9.5
DECEMBER	11.3	17.6	6.5	69.9	20.06	12.2
Moy	23.967	30.35	16.34167	34.80833	2.793333	14.08333

2014	T	TM	Tm	H	PP	V

JANUARY	12.5	19.3	6.3	55.9	0	8.9
FEBRUARY	15.6	22.9	8.3	36.8	0	12.5
MARCH	17.5	23.9	10.2	34.6	0.5	17.4
APRIL	23.8	31.2	15	22.2	0	12.9
MAY	28.5	35.3	20.4	22.6	13.97	18
JUNE	32.2	39.8	23.7	19.9	2.03	18.4
JULY	37.1	44.4	28.5	16.8	0	15.8
AUGUST	36.4	44.2	28.2	17.1	0	14
SEPTEMBER	33.3	40.7	25.8	21.2	0	14.9
OCTOBER	24.9	33	16.9	27.2	2.03	10.9
NOVEMBER	18.5	25.9	11.9	40.8	7.11	10.8
DECEMBER	12	19	6.2	54.2	6.1	9.4
	24.358	31.63333333	16.78333	30.775	2.645	13.65833
2015	**T**	**TM**	**Tm**	**H**	**PP**	**V**
JANUARY	10.8	18.4	4	45.1	0.76	10.6
FEBRUARY	12.4	18.7	6.8	41.8	22.09	17.1
MARCH	17.3	24.7	10	32.6	5.08	12.3
APRIL	24.3	31.8	16.1	21.9	0	17
MAY	29.5	37.1	20.5	17.5	0	16
JUNE	32.8	39.8	24.8	17.9	0	0.6
JULY	34.8	42	26.5	17.1	0	17.8
AUGUST	36.1	42.8	29.3	21.5	0	14.9
SEPTEMBER	30.9	37.9	23.6	29.1	1.27	13.2
OCTOBER	24.7	31.9	17.5	34.8	0	11.2
NOVEMBER	17.2	24.3	11	48.3	0	4.4
DECEMBER	11.7	20	5	55.2	0	4.4
Moy	23.542	30.78333333	16.25833	31.9	2.433333	11.625
2016	**T**	**TM**	**Tm**	**H**	**PP**	**V**
JANUARY	13.3	21.3	6.2	40.8	0	8.9
FEBRUARY	15.3	22.8	8.1	34.1	0	11.8
MARCH	17.8	25.8	9.4	24.8	2.03	12.2
APRIL	24.8	32.8	16.8	30	1.02	18.8
MAY	29.1	36.1	21.2	18.6	0	18.6
JUNE	33.6	41	25	17.3	0	18.2
JULY	35.5	42.6	27.4	16.3	0	15.7
AUGUST	34.4	41.3	26.9	19.5	0	15.1
SEPTEMBER	31.1	38	24.1	28.9	2.54	13.4
OCTOBER	26.4	34.1	19.1	33.8	3.05	13.5
NOVEMBER	17	24.2	10.2	41.9	0.76	7
DECEMBER	13.2	19.3	8.3	63	7.11	12.2
Moy	24.292	31.60833333	16.89167	30.75	1.375833	13.78333

2017	**T**	**TM**	**Tm**	**H**	**PP**	**V**
JANUARY	10	17.1	3.4	45.7	0.25	10.6

FEBRUARY	15.4	22.7	8.6	36.5	0	14.6
MARCH	18.9	25.8	11.6	31.6	21.08	15
APRIL	22.7	29.6	15	28.9	0.76	19
MAY	30.5	37.3	22.9	20.3	0	19.7
JUNE	33.4	40.1	25.5	19.2	0.25	16.4
JULY	35.6	42.7	27.2	15.4	0	14.08
AUGUST	35.4	42.8	27.1	16.5	0	14
SEPTEMBER	29.1	36.4	21.9	31.2	12.95	14.3
OCTOBER	22.5	29	16	42.8	23.12	10.1
NOVEMBER	15.6	22.6	9.3	49.6	14.48	9.8
DECEMBER	11	17.7	5.3	53.8	2.28	11.9
Moy	23.342	30.31666667	16.15	32.625	6.264167	14.12333
2018	**T**	**TM**	**Tm**	**H**	**PP**	**V**
JANUARY	12.6	20.2	5.9	44.3	0	12.2
FEBRUARY	13.2	19.5	7	45.6	5.33	11.9
MARCH	19.4	26.1	12	26.5	0	17.6
APRIL	23.4	30	16.1	26	0	17.9
MAY	27.6	34.8	20.1	26	5.08	19.7
JUNE	32.4	39.4	24.5	20.2	0	15.2
JULY	39.2	47.1	30.5	12	0	13.6
AUGUST	33.6	40.1	26.8	26.7	1.02	13.9
SEPTEMBER	31.7	38.1	24.9	28.1	10.92	15.9
OCTOBER	23.2	29.7	16.9	35.3	0	12.4
NOVEMBER	16.6	23.3	10.3	42.4	0.76	11
DECEMBER	11.8	19.9	5	50.3	0	7.8
Moy	23.725	30.68333333	2	31.95	1.925833	14.09167
2019	**T**	**TM**	**Tm**	**H**	**PP**	**V**
JANUARY	10.8	18.4	4	40.8	0	10.3
FEBRUARY	12	19.2	4.9	37.8	0	13.8
MARCH	16.9	24.2	9.2	33.5	4.07	14.4
APRIL	23.2	30.2	15.5	25.9	13.97	14.9
MAY	26.7	33.3	19	25	3.81	16.1
JUNE	35.3	42.6	26.6	13.9	0	17.5
JULY	37.4	44.5	28.8	13.8	0	13
AUGUST	36.9	43.5	29.7	17.8	0	13.3
SEPTEMBER	31.8	39.1	24	27.5	1.53	12.8
OCTOBER	24.2	31	17.2	35.8	2.03	10.4
NOVEMBER	16.2	23.3	9.3	37.3	0	11
DECEMBER	13.8	21.1	7.1	46.7	0	10.3
Moy	23.767	30.86666667	16.275	29.65	2.1175	13.15

2020	**T**	**TM**	**Tm**	**H**	**PP**	**V**
JANUARY	10.6	19	3.4	46.1	0	8
FEBRUARY	15	23.4	6.7	35.5	0	8.3

MARCH	18.9	25.8	11.3	33.3	2.03	16.4
APRIL	24.1	30.7	16.4	29	5.08	16.4
MAY	30	37.1	21.7	19.2	3.05	16.3
JUNE	33.7	40.6	25.5	17	0	14.5
JULY	36.1	42.7	28.1	17.2	0	14.2
AUGUST	36.1	43.2	27.7	16	0	11.6
SEPTEMBER	30.2	37.3	23	30.4	3.05	12.6
OCTOBER	22.8	29.6	15.6	33.6	0	12.2
NOVEMBER	18.1	24.6	11.4	42.5	0	8.8
DECEMBER	13.2	19.7	6.9	45.3	0	10.9
Moy	24.067	31.14166667	16.475	30.425	1.100833	12.51667
2021	**T**	**TM**	**Tm**	**H**	**PP**	**V**
JANUARY	13	20.7	15	36.6	0	9.2
FEBRUARY	16.2	22.7	9.8	31.7	0	15
MARCH	17.4	23.7	10.4	32	0	14.9
APRIL	24.1	30.7	16.4	24.4	0	16.7
MAY	29.2	35.8	21.8	25	2.79	14
JUNE	36.5	43	28.7	15.2	0	17
JULY	37.7	44.4	29	15.1	0	11.8
AUGUST	37.4	44.8	28.6	12.7	0	11.7
SEPTEMBER	34.2	41.4	26.3	18.9	1.02	13.8
OCTOBER	23.8	30.2	17.2	33	0	10.9
NOVEMBER	16.5	22.6	10.1	43.4	29.97	19.2
DECEMBER	11.9	8.3	6.4	54.7	0	7.5
Moy	24.825	30.69166667	18.30833	28.55833	2.815	13.475

Aabstract

الملخص:

تمت في هذه الدراسة محاكاة ثلاثية الابعاد للمبادل الحراري الارضي لغرض تحسين كفاءته في تكييف الجو خلال الفصلين الشتاء والصيف بمنطقة ورقلة، حيث اعتمدنا على دراسة سابقة مثبتة تجريبيا في تصميم وتفعيل النموذج.واستخدمنا طريقة طاقوشي لتخطيط التجارب وكان هذا باختيار اربعة عوامل مؤثرة في أداء المبادل واسناد ثلاثة قيم (مستويات) لكل عامل. أظهرت النتائج أن الحد الأقصى لفرق درجة الحرارة في الهواء بين المدخل ومنفذ EAHE حوالي 19.45 درجة مئوية و 17.77 درجة مئوية لشهر يناير ويوليو، في حين حوالي 2.44 درجة مئوية و 2.6 درجة مئوية لشهري أبريل وأكتوبر.

الكلمات المفتاحية:المبادل الحراري الهوائي الارضي ، محاكاة CFD ثلاثية الابعاد ، طريقة طاقوشي.

Abstract

In this study, a three-dimensional simulation of the geothermal heat exchanger was carried out in order to improve its efficiency in air conditioning during the winter and summer seasons in the region of Ouargla, based on a previous experimentally valid study in designing and validating the geothermal heat exchanger CFD model. Using Taguchi's method to plan experiments, and this was done by selecting four factors affecting the performance of the exchanger and assigning three values (levels) to each factor. The results show that the maximum temperature difference of air between the inlet and the outlet of the EAHE is around 19.45 °C and 17.77 °C for the months of January and July, while the minimum temperature difference between the air entering and leaving the EAHE is about 2.44°C and 2.6 °C for the months of April and October.

Key words: Ground air heat exchanger, 3D CFD simulation, Taguchi method,

Résumé

Dans cette étude, une simulation tridimensionnelle de l'échangeur de chaleur géothermique a été réalisée afin d'améliorer son efficacité en climatisation pendant les saisons d'hiver et d'été dans la région d'Ouargla, sur la base d'une étude antérieure valide expérimentalement dans la conception et la validation de Modèle CFD d'échangeur de chaleur géothermique. En utilisant la méthode de Taguchi pour planifier des expériences, cela a été fait en sélectionnant quatre facteurs affectant les performances de l'échangeur et en attribuant trois valeurs (niveaux) à chaque facteur. Les résultats montrent que la différence de température maximale d'air entre l'entrée et la sortie de l'EAHE est d'environ 19,45 ° C et 17,77 ° C pour les mois de janvier et juillet, respectivement, tandis que la différence de température minimale entre l'air entrant et sortant du EAHE est environ 2,44 ° C et 2,6 ° C pour les mois d'avril et octobre, respectivement.

Mots clés : Echangeur sol air, simulation CFD 3D, méthode Taguchi,